National Technical University of Athens

Civil Engineering school
MGroup - Computational Department of the Institute of Static Analysis
and Seismic Research lab -

Development and Testing of a Coupled Biphasic Numerical Model of Tumor Growth

Computational Mechanics Joint Post Graduate Course

by
Papas Christoforos Orestis

Supervised by
Papadopoulos Vissarion

16 November 2023

Contents

List of Figures

List of Tables

Abstract

This thesis focuses on the computational solution and validation of a sophisticated numerical model for simulating the tumor microenvironment (TME), emphasizing the interactions among cancer cell proliferation, oxygen transport phenomena, and the mechanical behavior of both tumor and host tissues. The primary objective is to develop and validate a reliable tool for understanding tumor dynamics, providing insights that can inform the design of more effective patient-specific treatments.

The mathematical model accounts for the biphasic nature of tumor tissues and their complex interactions with surrounding healthy tissues. The mechanical behavior is modeled using both linear and hyperelastic constitutive laws, while the transport phenomena are governed by coupled convection-diffusion-reaction partial differential equations for oxygen concentration and cancer cell population. These formulations include detailed representations of interstitial fluid flow, solid stress states, and the influence of tumor growth on tissue deformation. Spatial discretization is achieved using the Finite Element Method, while temporal discretization is performed with methods such as Newmark and Generalized-α. Coupling of the linear systems is accomplished with an advanced iterative solver. The methods developed are implemented in msolve and benchmarked against COMSOL to ensure accuracy and reliability.

The results highlight significant differences in mechanical responses and transport phenomena between tumor and host tissues, influenced by their inherent heterogeneity. Detailed simulations provide valuable information on growth patterns, stress distributions, and oxygenation levels within the Tumor Micro Environment (TME), contributing to a deeper understanding of the mechanisms driving cancer progression.

Overall, this thesis underscores the crucial role of computational modeling in medical research and serves as a foundation for refining clinical research parameters for patient-specific treatments. Future integration with stochastic and AI tools, along with the utilization of MRI data and advanced HPC platforms, will further improve the accuracy and applicability of these simulations in personalized cancer therapy.

Chapter 1

Introduction

Cancer is a complex and multifaceted disease that arises from the abnormal growth and division of cells in the body. It occurs in any tissue or organ of the body and can spread to other parts of the body through the bloodstream or lymphatic system. There are many different types of cancer, each with its own set of symptoms, risk factors, and treatment options. Cancer remains a major global health concern. In 2020, approximately 19.3 million new cancer cases and almost 10 million cancer deaths were reported worldwide [15, 36]. Looking ahead, the number of new cancer cases and deaths is expected to rise significantly. By 2030, the World Health Organization predicts a 69% increase in new cancer cases, reaching 21 million, and a 72% increase in cancer deaths, reaching 13 million [5]. Another projection estimates around 26 million new cancer cases and 17 million cancer deaths per year by 2030. This increase is attributed largely to population growth and aging, with the most significant impacts expected in low- and medium-resource countries [35].

1.1 Etiology of Cancer

Cancer is a complex disease with multiple etiological factors that interact to initiate and promote tumor development. While the specific cause remains unknown, it is widely accepted that cancer arises from a combination of genetic and environmental factors. Advances in molecular and genetic technologies have provided a better understanding of the genetic alterations that occur in tumor cells, but the precise interplay between genetic and environmental factors that lead to cancer development is not yet fully understood.

1.1.1 Genetic & Environmental Factors

Cancer arises from a complex mix of genetic mutations and environmental factors. Genetic changes disrupt normal cell growth, leading to cancer, with these mutations varying widely

across different cancers [34, 14, 1]. Environmental factors, including lifestyle, occupational hazards, and exposure to substances like tobacco and radiation, significantly increase cancer risk [7, 19, 28]. Social determinants like socio-economic status also play a crucial role, with lower-income groups facing higher exposure to carcinogens and limited access to healthcare [12, 19]. Additionally, non-social elements like chronic inflammation, certain viruses, and psychological stress contribute to cancer development, underlining the disease's multifaceted nature [7, 28].

1.2 Tumor Growth Modeling

Tumor growth is a multifaceted phenomenon that involves interactions among tumor cells, surrounding tissues, and the micro-environment. Traditional experimental and clinical methods for studying tumor growth are often limited by various factors such as ethical concerns, cost, and practical feasibility. Mathematical modeling offers a complementary approach that allows for a systematic investigation of tumor growth dynamics in a controlled and quantitative manner. By developing a numerical model that simulates tumor growth, we aim to gain insights into the underlying mechanisms and interactions involved in tumor growth, which can inform the design of more effective cancer therapies. It is obvious that cancer treatment as well as prediction is a major challenge for the human race and significant effort from a wide range of scientific domains is needed. Mathematical modeling offers a complementary approach that allows for a systematic investigation of tumor growth dynamics in a controlled and quantitative manner. In the era of hexa-scale computing and artificial intelligence, a rigorous, high-fidelity mathematical model can be solved for huge sets of parameters and various useful stochastic insights can be provided.

1.3 Objective of the Thesis

The primary objective of this thesis is to document the development and validation of a sophisticated numerical model designed to simulate the microenvironment and growth of a biphasic tumor. This model, developed within MSolve, focuses on capturing the intricate dynamics of tumor growth and interaction within its microenvironment. MSolve, an open-source, multiphysics platform, has been developed by the MGroup Lab at the ISAAR School of Civil Engineering, NTUA.

Central to this objective is the advancement of the mathematical modeling aspects of tumor growth. The model incorporates a comprehensive approach, accounting for the biphasic

nature of tumor tissue and the complex interactions within the tumor microenvironment. This includes detailed simulations of mechanical and transport phenomena on tumor growth and development.

Ultimately, the thesis aims to contribute to the field of cancer research by offering a reliable and comprehensive tool for understanding tumor dynamics. The insights gained from this research are expected to inform the development of novel cancer therapies, enhancing the efficacy of treatment approaches and improving patient outcomes. This research underscores the crucial role of advanced computational modeling in deciphering the complexities of cancer and paves the way for future innovations in cancer therapy.

Chapter 2

Mathematical Modeling

2.1 Introduction

The microenvironment is modeled as a quartersphere tumor tissue embedded in a cube representing the healthy tissue. Both tissue types are biphasic consisting of a solid and a fluid phase with different material properties. Due to this type of solid-fluid interaction the medium is considered as porous. By appplying properly manipulated mathematical formulations, such as augmented versions of the well established mass/energy/momentum flux equations that respect the domain physics and heterogeneities, the transport phenomena and the kinematics of the system break down to a coupled system of partial and differential equations which can be affected by various parameters. Healthy and tumor tissues are well known to be heterogeneous, leading to variations in mechanical properties like porosity and permeability, that can cause non-uniform flows between regions. The aforementioned non-uniform mechanical properties of the system are accounted for with varying equation forms and constant values. In the following sections of this chapter a thorough description of the mathematical model is presented containing all the equations involved, their parameters and the ways they infer with each other.

2.2 Mechanical Behaviour of Biphasic Tumor

2.2.1 Fluid Phase

The motion of the interstitial fluid, that fills the spaces between the cells, provides a medium for the dialution and exchange of nutrients, treatment agents, and various molecules. In the following subsections the phenomena resulting from the fluid flux within the porous matrix are examined.

2.2.1.1 Fluid Pressure - p

The accurate description of the pressure field p of the TME is of major importance as it affects the interstitial fluid flow as well as the stress state of the solid phase by adding hydrostatic components to the stress tensor. Darcy's law for porous media describes the fluid velocity vector $\boldsymbol{v_f}$ as a function of the gradient of p_i [6], the hydraulic conductivity of the interstitial space [32] and the velocity of the solid phase $\boldsymbol{v_s}$ and is expressed as follows:

$$\boldsymbol{v_f} = -k_{th}\nabla p_i + \boldsymbol{v_s} \tag{2.1}$$

The generalized differential form of the steady-state continuity equation for a locally non conserved quantity is deduced by the divergence theorem :

$$\boldsymbol{\nabla} \cdot \boldsymbol{u_f} = Q \tag{2.2}$$

while Q denotes the flux entering from the blood vessels into the tissue minus the fluid flux exiting through lymphatic vessels [31]:

$$Q = L_p S_v(p_v - p_i) - L_{pl} S_{vl}(p_i - p_l) \tag{2.3}$$

After some routine mathematical manipulation the synthesis of the principles of porous fluid flow (2.1), and mass conservation (2.2) yield the steady-state fluid transport equation:

$$-k_{th}\nabla^2 p_i = Q - \nabla \cdot (\boldsymbol{v_s}) \tag{2.4}$$

The Laplacian (diffusion) operator quantifies the curvature of the pressure field and represents the driving force of flow due to pressure gradients. In areas where there are sharp pressure changes, for example near a growing tumor, the term becomes significant and vice versa. The $\boldsymbol{\nabla}\cdot$ vector operator is the divergence of a vector field and quantifies the net outflow (or inflow) of a vector field from an infinitesimal volume around a given point. A positive divergence indicates a source (or outflow) behavior, while a negative divergence signifies a sink (or inflow) behavior. In the context of the TME, this equation captures how fluid is conserved as it moves through the porous tissue. The divergence of the solid phase velocity captures the influence of the solid phase (cells, extracellular matrix etc) onto the fluid motion, since mechanical deformations exert pressure onto the surroundings. :
All the model constants involved in Equation(2.4) that capture the heterogenous / non- heterogenous hydraulic properties of the tissue and the pressures in the vascular and lymphatic systems.

Variable	Unit	Description
p_i	kPa	Fluid Phase Pressure (Dependent Variable)
$\boldsymbol{v_s}$	m/s	Solid Phase Velocity (Communicated Dependent Variable Derivative)
k_{th}	m^2/(kPa·s)	Fluid Phase Hydraulic Conductivity
Q	1/s	Source due to flow between blood vessels and the tissue and drainage through lymphatic vessels.
L_p	m/(kPa·s)	Blood Vessel Walls Hydraulic Conductivity
S_v	1/m	Vascular Density (Blood vessels per unit volume of tissue).
p_v	kPa	Vascular Pressure.
p_l	kPa	Lymphatic Pressure
$L_{pl}S_{vl}$	1/(kPa·s)	Lymphatic vessel permeability

Table 2.1: Fluid Transport Equation Variables and Parameters

2.2.1.2 Hydrostatic Pressure

Consider a stress state where the stress tensor $\boldsymbol{\sigma}$ is described as follows:

$$\boldsymbol{\sigma} = \begin{bmatrix} p & & \\ & p & \\ & & p \end{bmatrix} = p\boldsymbol{\delta} \Rightarrow \sigma_{ij} = p\delta_{ij}$$

By transforming the second order tensor to a coordinate system $OX_1^{'}$, $OX_1^{'}$, $OX_1^{'}$:

$$\sigma_{ij}^{'} = Q_{ik}Q_{jl}\sigma_{kl} = Q_{ik}Q_{jl}(p\delta_{kl}) = Q_{ik}Q_{jk}p = p\delta_{ij}$$

it can be easily observed that the normal components of the stress tensor σ remain the same, while the shear components are equal to 0 for any arbitrarily chosen coordinate system. For $p < 0$ or $p > 0$ the state is described as hydrostatic tension and hydrostatic pressure correspondingly.

In the case of tumor modeling the hydrostatic pressure is a product of the fluid flow as described by Equation(2.4) and the fluid pressure stress tensor is [2]:

$$\sigma_{ij}^{f} = -p_i\delta_{ij} = -p_i\boldsymbol{I} \tag{2.5}$$

2.2.2 Solid Phase

2.2.2.1 Solid Phase Deformation

The kinematic description of the solid phase is governed by the laws of classical mechanics. The description of the deformation of a solid body requires the use of a "reference geometry" or "reference state." In this context, a reference state refers to the initial or undeformed state of a material body or system and serves as a fundamental framework for measuring and describing subsequent deformations and changes in the solid body. It provides a fixed point of reference from which all deformations are evaluated and enables the formulation of mathematical models and analysis techniques to study the behavior of the material under various loading and boundary conditions.

Consider a random point within the material body, characterized by its unique initial position vector $\boldsymbol{X}$ and its final position vector $\boldsymbol{x} = x(\boldsymbol{X}, t)$. Here, $x(\boldsymbol{X})$ represents the mapping of the field that describes the final state of the solid body relative to its initial state.

The final position vector $x(\boldsymbol{X})$ function is assumed to be continuous and differentiable, enabling a complete description of the motion and deformation of the solid body. By comparing the initial and final positions, we can quantify and analyze the extent and nature of deformation experienced by the material. The displacement of the point is given by :

$$\boldsymbol{u}(\boldsymbol{X}, t) = \boldsymbol{x}(\boldsymbol{X}, t) - \boldsymbol{X} \tag{2.6}$$

The elastic deformation gradient tensor is :

$$\boldsymbol{F} = \frac{\partial \boldsymbol{x}(\boldsymbol{X}, t)}{\partial \boldsymbol{X}} = \boldsymbol{x}\boldsymbol{\nabla} \tag{2.7}$$

while the kinematic description of a solid tumor in terms of deformation can be decomposed into two components, a local, non-stress-generating, volumetric growth component $\boldsymbol{F_g}$ that accounts for the growth of the tumor with respect to the initial undeformed state and the elastic component $\boldsymbol{F_e}$ that accounts for the mechanical interactions of the tumor with the surrounding normal tissue [30] :

$$\boldsymbol{F} = \boldsymbol{F_e}\boldsymbol{F_g} \tag{2.8}$$

The growth component is set to be homogeneous and isotropic [29]

$$\boldsymbol{F_g} = \lambda_g \boldsymbol{I} \tag{2.9}$$

where λ_g is the growth stretch ratio, which accounts for cancer cell proliferation, as defined in Equation(2.24). The elastic component of the deformation gradient tensor is :

$$\boldsymbol{F_e} = \boldsymbol{F}\boldsymbol{F_g^{-1}} \tag{2.10}$$

The Cauchy - Green strain tensor $\boldsymbol{C}_e$ is :

$$\boldsymbol{C_e} = \boldsymbol{F_e}^T\boldsymbol{F_e} \tag{2.11}$$

while the Green-Lagrange strain tensor $\boldsymbol{\epsilon}$ can be written in terms of $\boldsymbol{C_e}$:

$$\boldsymbol{\epsilon} = \frac{1}{2}(\boldsymbol{C_e} - \boldsymbol{I}) \tag{2.12}$$

It should be noted that the definition of the Green-Lagrange strain tensor is based on derivatives with respect with the initial, undeformed coordinates of the particles.

2.2.2.2 Solid Phase Stress

Heterogenous mechanical stresses developed during tumor growth play a central role in cancer proliferation since they lead to non-uniform compression of the intratumoral blood vessels, drastically reducing the supply of nutrients and treatment[9][20][21] and leading to hypoxia and necrosis [16][27][31]. The stress state of the solid phase will be described based on the continuum mechanics laws. The Momentum Conservation Law states that the total sum of forces applied to a solid body is equal to the spatial integral of the product of the body's density and its acceleration within the spatial domain it occupies. In other words, when external forces act on a solid body, the combined effect of these forces can be determined by calculating the integral of the density-acceleration product across the entire volume of the body. This principle highlights the fundamental relationship between forces, density, and acceleration and for an aribitarily chosen part of the solid body $\mathbb{B}'$ with boundary $\partial\mathbb{B}'$ takes the form [2]:

$$\int_{\mathbb{B}'} \boldsymbol{t}dS + \int_{\mathbb{B}'} \rho(\boldsymbol{b} - \boldsymbol{a})dV = \boldsymbol{0} \tag{2.13}$$

where $\boldsymbol{a}$ is the acceleration, $\boldsymbol{b}$ is the vector of field forces (gravity, electromagnetic etc), ρ is the density. After some routine mathematical manipulation the partial differential equations of motion are derived:

$$\boldsymbol{\nabla} \cdot \boldsymbol{\sigma} + \rho\boldsymbol{b} = \rho\boldsymbol{a} \tag{2.14}$$

In the case of the tumor micro-environment, the rate of change of the velocity and the effect of body forces are neglected. The equation of motion describing a solid tumor can be expressed as follows:

$$\boldsymbol{\nabla} \cdot \boldsymbol{\sigma} = \mathbf{0} \tag{2.15}$$

According to the biphasic theory for soft tissues[24] The isotropic hydrostatic fluid pressure components described in Equation((2.5)) acts on the solid stress tensor, producing an equal force in all normal directions and contributes directly to the total stress state of the solid phase.Combining Equations (2.15) and (2.4) produces the final strong form of the solid phase stress state where the intricate coupling of the fluid pressure and solid stresses can be observed:

$$\boldsymbol{\nabla} \cdot (\boldsymbol{\sigma^s} - \boldsymbol{\sigma^f}) = \boldsymbol{\nabla} \cdot (\boldsymbol{\sigma^s} - p_i \boldsymbol{I}) = \mathbf{0} \tag{2.16}$$

The mechanical behavior of the tissue is simulated with a hyper-elastic material while the Cauchy stress tensor $\boldsymbol{\sigma^s}$ is given by[33]:

$$\boldsymbol{\sigma^s} = J_e^{-1} \boldsymbol{F}_e \frac{\partial W}{\partial \boldsymbol{F}_e^T} \tag{2.17}$$

where $J_e = \det \boldsymbol{F_e}$ and W is the modified neo-Hookean strain energy density function for a nearly incompressible hyper-elastic material[37][38][39]:

$$W = \frac{1}{2}\mu(-3 + II_1) - p(J_e - 1) - \frac{p}{2k} \tag{2.18}$$

with μ, k being the shear and bulk moduli of the material, $II_1 = I_1 J_e^{-2/3}$, $I_1 = tr\boldsymbol{C^e}$ the first and second invariants of the elastic Cauchy-Green deformation tensor while p is Lagrange multiplier enforcing material constraints.

Since the material is non-liner the second Piola-Kirchhoff tensor is introduced that relates the stress state of the current configuration to the current stress-state:

$$\boldsymbol{S} = J\boldsymbol{F}^{-1} \cdot \boldsymbol{\sigma} \cdot \boldsymbol{F}^{-T} \tag{2.19}$$

$$S_{il} = J \frac{\partial X_i}{\partial x_k} \frac{\partial X_l}{\partial x_m} \sigma_{km} \tag{2.20}$$

2.2.3 Growth Stretch Ratio

In the study of tumor progression, understanding the volumetric growth stretch ratio λ_g, is of paramount importance. It represents the relative change in the tumor volume over time and various mathematical formulations have been developed, all of whom take into account the oxygen concentration and the proliferation of one or more cancer cell types. The affect of λ_g in the deformation of the solid matrix can be seen in (2.9) as it appears in the diagonal of the elastic non-stress- deformation gradient tensor F_g adding external strains.
The following formulation considers the ratio of the population of normal T_{SC}, stem-cell-like T_I and induced T_{CC} cancer cells over the total population oc cancer cells T_{tot}, as well as their corresponding proliferation / degradation rates S_T^c, S_I^C, $S_{C_{SC}}^c$:

$$\frac{d\lambda_g}{dt} = \frac{1}{3}\left(\frac{T_{CC}}{T_{tot}}S_T^c + \frac{C_{SC}}{T_{tot}}S_{C_{SC}}^c + \frac{I}{T_{tot}}S_I^C\right)\lambda_g \tag{2.21}$$

Another model for λ_g is proposed in [25] where the direct effect of solid stresses on reducing cancer cell proliferation and the effect of drug delivery are also considered. The dependence of the growth rate on the local oxygen concentration G is measured experimentally as [8] as follows:

$$G = \frac{k_1 c_{ox}}{k_2 + c_{ox}} \tag{2.22}$$

Equations like (2.22) are known Michaelis - Menten equations in enzyme kinetics and they represent the saturation curve. In the context of the TME it implies that the tumor growth rate increases with oxygen concentration initially but plateaus as the oxygen concentration continues to rise. O_2 plays a crucial role in tumor growth, as it fuels cellular metabolism and proliferation. Higher concentration values promote faster growth rates while low (hypoxic conditions) lead to slower growth rates even cellular death.
The mathematical formulation for λ_g is [30][22][23][37]:

$$\frac{d\lambda_g}{dt} = \frac{1}{3}G(1 - \beta\bar{\sigma^s})S_f\Phi^C(1 - \Phi^C)\lambda_g \tag{2.23}$$

where $\bar{\sigma^s} = tr\sigma^s/3 = (\sigma_{rr} + \sigma_{\theta\theta} + \sigma_{\phi\phi})/3$ is the average of the Cauchy stress tensor of the solid phase, Φ^C is the volume fraction of the solid tumor phase and β is a constant that describes the dependence of growth on solid stress. It is further assumed that only compressive solid stress inhibits tumor growth [10][17] therefore, the term $(1 - \beta\bar{\sigma^s})$ is positive but less than unity when the bulk stress is compressive and equal to unity when the bulk stress is tensile. Finally, to account for the effect of drug delivery, the fraction of survived cells S_f is included,

so that in the absence of drugs it is equal to unity.
In the context of this thesis the development of the a simplified version of (2.23) is implemented. The equation considers only normal cancer cells T_{CC} and G:

$$\frac{d\lambda_g}{dt} = \frac{1}{3}\frac{k_1 c_{ox}}{k_2 + c_{ox}} T_{CC} \tag{2.24}$$

Its should be noted that (2.24) is solved explicitly in the tumor domain, while $\lambda = 1$ for the healthy domain.

Variable	Unit	Description
λ_g	1	Growth Stretch Ratio (Dependent Variable)
c_{ox}	mol/m^3	Oxygen Concentration (Communicated Dependent Variable)
T_{CC}	1	Cancer Cell Population (Communicated Dependent Variable)
k_1	1/s	Growth rate parameter
k_2	mol/m^3	Growth rate parameter

Table 2.2: Growth Stretch Ratio Variables and Parameters

2.3 Nutrients & Cell Transport Phenomena

Understanding the balance, interplay, and spatial/temporal evolution of the cellular and nutrient transport phenomena provides insights into how cells and nutrients dynamically interact and navigate through the heterogeneous tumor micro-environment (TME). It allows for the exploration and prediction of phenomena like nutrient depletion zones, cell migration, and the emergence of concentration gradients, which are crucial in investigating tumor progression, cellular behavior, and response to treatments in a spatiotemporally evolving system. These phenomena are modeled with the general form of the Convection-Diffusion-Reaction Equation :

$$\alpha(\boldsymbol{x})\frac{\partial \boldsymbol{\Phi}(\boldsymbol{x},t)}{\partial t} = \beta(\boldsymbol{x})\boldsymbol{\nabla}^2\boldsymbol{\Phi}(\boldsymbol{x},t) - \gamma(\boldsymbol{x})\nabla\cdot[\boldsymbol{v}(\boldsymbol{x},t)\boldsymbol{\Phi}(\boldsymbol{x},t)] + \delta(\boldsymbol{x})\boldsymbol{\Phi}(\boldsymbol{x},t) + \epsilon(\boldsymbol{x}) \tag{2.25}$$

- $\alpha(\boldsymbol{x}), \beta(\boldsymbol{x}), \gamma(\boldsymbol{x}), \delta(\boldsymbol{x}), \epsilon(\boldsymbol{x})$ are the spatially varying coefficients of the PDE that account for the heterogeneities in the different regions of the TME. From now on they will be denoted as: $\alpha, \beta, \gamma, \delta, \epsilon$.

- The temporal derivative term represents the rate of change of $\boldsymbol{\Phi}$ over time, accounting for the transient behavior of the system and significantly influencing the numerical stability

of the numerical scheme. In the context of the current mathematical model α is set equal to 1.

- The diffusion of $\mathbf{\Phi}$ is described by the Laplace operator and describes the passive transport due to spatial gradients. Diffusion is linked with the molecular properties of the medium and occurs due to the natural tendency of systems to equilibrate to high entropy states which correspond to a uniform, more probable, distribution of $\mathbf{\Phi}$. It is associated with the random motion of particles (Brownian motion) and creates fluxes from regions of higher values of the dependent variable to those of lower until an equilibrium state is achieved. In biological and physical systems, diffusion is a pivotal transport mechanism, particularly apparent in cellular environments where nutrient, mechanical properties or cell gradients occur.

- The convection term $(-\gamma(\boldsymbol{x})\nabla\cdot[\boldsymbol{v}(\boldsymbol{x},t)\mathbf{\Phi}(\boldsymbol{x},t)])$ involves the bulk movement, potentially driven by pressure gradients, flow fields, or other macroscopic transport mechanisms. In the case of the TME convective transport occurs due to the bulk motion of the solid matrix and the interstitial fluid as described in previous sections. Convection dominated flows are well known to cause numerical instabilities for $(Pe > 1)$, where $P = (UL)/\beta$ is the Pecklet number of the flow and depends on the ratio of the characteristic length L and velocity U of the flow over the diffusion coefficient β.

- The reaction term $R(\mathbf{\Phi}) = \delta\mathbf{\Phi} + \epsilon$ represents the internal sources, sinks, or any other interactions of the quantity $\mathbf{\Phi}$, abstracting various possible physical or biological phenomena. In diverse contexts, this might encapsulate aspects such as decay, generation, or transformation of $\mathbf{\Phi}$ due to intrinsic properties of the medium or external inputs. The specific form of this term is often dictated by the nature of the processes being modeled, and it might embody a range of kinetics, from linear to nonlinear forms, each with its own implications and interpretational nuances. This term serves as a crucial connector, linking the transport processes described by the other terms in the equation with the local behavior and properties of the system, thereby enriching the model with the capability to simulate a spectrum of scenarios and behaviors.

2.3.1 Oxygen Transport

Oxygen transport phenomena are paramount in the TME. Impaired blood perfusion in the tumor region limits the delivery of drugs, immune cells, and oxygen. Reduced oxygen concentration, known as hypoxia, is considered a hallmark of the abnormal tumor micro-environment,

inducing immunosuppression. Conversely, high oxygen supply can fuel tumor growth and proliferation. Thus, precise modeling of oxygen transport phenomena is vital for understanding and predicting the spatial-temporal evolution of oxygen concentration within tumor and host tissues, enabling insightful predictions of hypoxic regions, influencing therapeutic response, and tumor progression. Further incorporation of factors like angiogenesis, necrosis, and therapeutic intervention can augment the model, enhancing its predictive capabilities and biological fidelity.

The mathematical modeling of O_2 concentration is achieved by the transient convection-diffusion-reaction equation[30][22]. Oxygen diffusion through the interstitial pores of the medium, due to concentration gradients, is described by Fick's law. Diffusivity varies between healthy and tumor tissues, with the latter being less diffusive. Additionally, a convective transport of oxygen occurs due to the bulk motion of the interstitial fluid. As described above in Equation (2.1), the flow velocity is affected by the fluid pressure gradients and the divergence of the solid matrix velocity field. The consumption of O_2 due to cancer cell proliferation is localized to the tumor region and is modeled using a non-linear Michaelis-Menten kinetics-type equation. This model regulates the rate of oxygen consumption, ensuring it adheres to saturation limits and illustrates the competitive uptake of oxygen by tumor cells in an environment deprived of nutrients. Both tumor and host regions utilize a shared source term to describe the exchange of oxygen between blood vessels and tissues, encapsulating the process of oxygen delivery and leakage from the vasculature to the interstitial space, which is influenced by both the permeability of vessel walls and vascular density. The modified versions of Equation (2.25), describing the aforementioned processes, are as follows:

$$\frac{\partial c_{ox}}{\partial t} + \nabla \cdot (c_{ox}\boldsymbol{v_f}) = D_{ox}\nabla^2 c_{ox} - \frac{A_{ox}c_{ox}}{c_{ox}+k_{ox}}T_{CC} + P_{er}S_v(c_{iox} - c_{ox}) \tag{2.26}$$

$$\frac{\partial c_{ox}}{\partial t} + \nabla \cdot (c_{ox}\boldsymbol{v_f}) = D_{ox}\nabla^2 c_{ox} + P_{er}S_v(c_{iox} - c_{ox}) \tag{2.27}$$

The dependent variables and coefficients involved in the above equations are:

2.3.2 Cancer Cell Proliferation

The accurate modeling and analysis of cancer cell proliferation within the tumor microenvironment (TME) stand as pivotal in comprehending tumor evolution and progression. Proliferation of cancer cells tends to decrease vessel diameter due to the compression of tumor vessels, thereby not only physically modifying the TME but also impacting nutrient and oxygen supply, which subsequently influences further tumor development. The functional

Variable	Unit	Description
c_{ox}	mol/m^{3}s	Oxygen concentration (dependent variable)
T_{CC}	1	Concentration of tumor cells
$\boldsymbol{v_f}$	m/s	Velocity vector of the fluid phase
D_{ox}	m^2/s	Diffusion coefficient of oxygen
A_{ox}	mol/m^{3}s	Maximal oxygen uptake rate by the tumor cells
P_{er}	m/s	Permeability of oxygen across tumor vessel walls
S_v	m^2/s	Vascular Density
c_{iox}	mol/m^3	Initial Oxygen Concentration in the blood vessels
k_1	1/s	Growth rate parameter
k_2	mol/m^3	Growth rate parameter

Table 2.3: Oxygen Concentration Equation Variables And Parameters

vascular density within the TME is determined by several variables: the hyper-permeability of blood vessels, the compression of vessels by proliferating cancer cells, prevailing solid stress levels, and the endothelial cell density.

The population balance of Cancer Cells (CC_s) is intricately linked to tumor perfusion and oxygenation, augmenting with an elevation in the oxygen level. The mathematical modeling of cancer cell proliferation is expressible through a Partial Differential Equation (PDE), exemplified below:

$$\frac{\partial T_{CC}}{\partial t} + \nabla \cdot (T_{CC}\boldsymbol{v_s}) = \frac{k_1 c_{ox}}{k_2 + c_{ox}} T_{CC}\lambda_g \tag{2.28}$$

The involved dependent variables and parameters are presented in Table 2.4

This PDE establishes a relationship amidst local oxygen concentration, the velocity field of the solid phase (comprising cancer cells), and the proliferation rate of the cancer cells. It enables exploration of how fluctuations in oxygen concentration, mediated via both convective and diffusive transport, can impact the spatial-temporal evolution of the tumor cell population within the TME. This modeling can act as a foundational component for the development of comprehensive, bio-physically detailed tumor models, and provides a platform to probe therapeutic strategies targeting tumor growth and proliferation.

Variable	Unit	Description
T_{CC}	1	Concentration of tumor cells (Dependent Variable)
c_{ox}	mol/m^{3}s	Oxygen concentration (Communicated Dependent Variable)
λ_g	1	Growth Stretch Ratio (Communicated Dependent Variable)
$\boldsymbol{v_s}$	m/s	Solid Phase Velocity (Communicated Dependent Variable Derivative)
k_1	1/s	Growth rate parameter
k_2	mol/m^3	Growth rate parameter

Table 2.4: Cancer Cell Population Equation Variables And Parameters

2.4 Summary

The mathematical model described in the previous sections has strong coupling connections between the 5 differential equations, which can be described as follows : The interstitial fluid pressure is affected by the divergence of the solid phase velocity field and affects the solid phase by adding hydrostatic components to the stress state. The divergence of the velocity fields of the solid and fluid phases are responsible for the convective flows of cancer cells and oxygen correspondingly. Cancer cell transport is included in the growth stretch ratio equation and the non-linear source term of oxygen transport, while oxygen supply plays a major role in the genesis of cancer cells since it is included in the source. The effect of oxygen is also very important in the growth stretch ratio of the solid phase, which affects the elastic deformation gradient tensor $\boldsymbol{F}$.

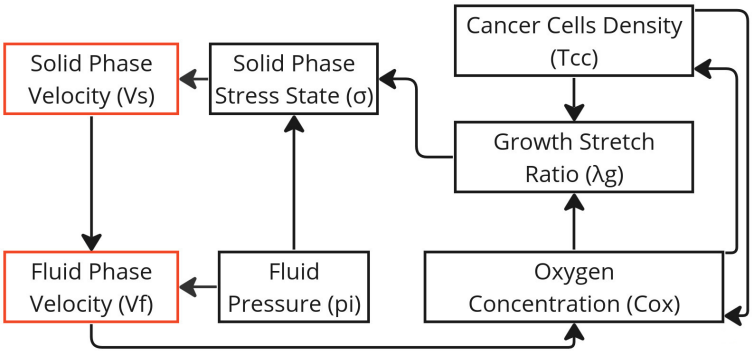

Figure 2.1: Equation Coupling Flow Chart

Chapter 3

Discretization in the Physical Space Domain

3.1 Introduction

This chapter aims to present the spatial discretization of equations (2.16), (2.4), (2.27), (2.26) and (2.28) as shown in Chapter 3 with the implementation of the Finite Element Method. This section contains information regarding the weak form formulations of the hyperelastic solid phase and the variations of the Convection-Diffusion-Production equation, as well as information about the discrete computational domain that represents the TME and the elements used.

3.2 Finite Element Discretization

The spatial discretization of the equations that govern the TME is achieved by the Finite Element Method, a powerfull numerical method, applicable to a vast array of physical problems that involve complicated physics, geometry and boundary conditions. The continous physical space is viewed as a collection of smaller sumbdomains (finite elements), consisted by discrete points (nodes). Each element is viewed as an independent domain by itself and it must satisfy the differential equation. The governing differential equation is approximated by the Galerkin variational method and it is viewed as a collection of simple algebraic polynomials, that are continous at the connecting nodes of neighbouring elements.
The basis of the displacement-based finite element analysis performed to calculate the response of the solid phase is the principle of virtual work. This principle states that the equilibrium of a solid body requires that for any compatible small virtual displacements imposed on the body while in equilibrium, the total internal virtual work is equal to the total external virtual work. In the examined case there is absence of external, body and inertial

forces so the corresponding virtual work of the first two should be zero, but for completness purposes they will be included in the following mathematical formulations. Consider any arbitrarily chosen continuus virtual displacements $\hat{u}_i$ satisfying $\hat{u}_i = 0$ at the boundaries of a solid body $\mathbb{B}'$. The governing equilibrium equation is:

$$\sigma_{ij,j} + f_i^B = 0 \tag{3.1}$$

3.2.1 Elastic solid phase

All the formulations that will be shown in this subsection are based on the assumption of linear elastic material, small displacements and small strains. Calculate the virtual work by multiplying (3.1) with the virtual displacements and integrate over the initial body volume:

$$\int_V \left(\sigma_{ij,j} + f_i^B\right) \hat{u}_i dV = 0 \tag{3.2}$$

where f_i^B is the applied body force field. In order for the above equation to be satisfied, for any arbitrarily chosen $\hat{\boldsymbol{u}}_i$ the quantity in the parentheses should be equal to 0. Integrate by parts:

$$\int_V \left[\left(\sigma_{ij}\hat{u}_i\right)_{,j} - \sigma_{ij}\hat{u}_{i,j} + f_i^B\hat{u}_i\right] dV = 0 \tag{3.3}$$

Apply Gauss theorem to convert body integral to surface and explicitly introduced natural (Neumann) boundary conditions to the principle of virtual displacements:

$$\int_V \left(-\sigma_{ij}\hat{u}_{i,j} + f_i^B\hat{u}_i\right) dV + \int_{S_f} f_i^S\hat{u}_i^S = 0 \tag{3.4}$$

Since $\sigma_{ij} = \sigma_{ji}$:

$$\sigma_{ij}\hat{u}_{i,j} = \sigma_{ij}\left[\frac{1}{2}\left(\hat{u}_{i,j} + \hat{u}_{j,i}\right)\right] = \sigma_{ij}\hat{\epsilon}_{ij} \tag{3.5}$$

we finally obtain the weak form of the steady state momentum equation:

$$\int_V \sigma_{ij}\hat{\epsilon_{ij}} dV = \int_V f_i^B\hat{u}_i dV + \int_{S_f} f_i^S\hat{u}_i^S dS = 0 \tag{3.6}$$

In Finite Method Analysis $\mathbb{B}'$ is approximated as the assemblage of M discrete finite elements. The governing equation (3.1) must be satisfied at all elements and the coordinate system can be chosen conviniently. We assume that the displacement field of every element e can be approximated as follows:

$$\boldsymbol{u}^e = \boldsymbol{N}^e\hat{\boldsymbol{u}}^e \tag{3.7}$$

where $\boldsymbol{N}^e$ is a matrix that contains the displacement interpolation polynomials, the so-called shape functions and $\hat{\boldsymbol{u}}^e$ is the vector containing the degrees of freedom of all n element nodes:

$$\hat{\boldsymbol{u}}_i(x,y,z) = \left\{ \begin{array}{c} u_{x,i}(x,y,z) \\ u_{y,i}(x,y,z) \\ u_{z,i}(x,y,z) \end{array} \right\} \Rightarrow \hat{\boldsymbol{u}} = \left\{ \begin{array}{c} u_{x,i} \\ u_{y,i} \\ u_{z,i} \end{array} \right\} \Rightarrow \hat{\boldsymbol{u}}^e \left\{ \begin{array}{c} \hat{\boldsymbol{u}}_0 \\ \vdots \\ \hat{\boldsymbol{u}}_i \\ \vdots \\ \hat{\boldsymbol{u}}_n \end{array} \right\}, i \in [0,n] \tag{3.8}$$

Strains are calculated based on the assumption of Equation (3.7) by properly calculating the gradients of $\boldsymbol{N}$:

$$\boldsymbol{\epsilon} = \boldsymbol{B}^e \hat{\boldsymbol{u}}^e$$

while stresses are calculated according to the constitutive matrix $\mathfrak{C}$ as follows:

$$\boldsymbol{\sigma} = \mathfrak{C}^e \hat{\boldsymbol{u}^e} \tag{3.9}$$

The response of the system is calculated by assembling the sum of all elements as follows:

$$\hat{\tilde{\boldsymbol{u}}}^T \left[\sum_{e=0,M} \int_{V^e} \boldsymbol{B}^{eT} \boldsymbol{C}^e \boldsymbol{B}^e dV^e \right] \hat{\boldsymbol{u}} = \hat{\tilde{\boldsymbol{u}}}^T \left[\left\{ \sum_{e=0,M} \int_{V^e} \boldsymbol{N}^{eT} \boldsymbol{f}^{B^e} dV^e \right\} + \left\{ \sum_{e=0,M} \int_{S^e} \boldsymbol{N}^{eT} \boldsymbol{f}^{S^e} dV^e \right\} \right] \tag{3.10}$$

To obtain the system of equations of the response, we apply the principle of virtual displacements n times imposing unit virtual displacements in turn for all components of $\hat{\tilde{\boldsymbol{u}}}^e = \boldsymbol{e}_1 ... \boldsymbol{e}_n$ and finally Equation (3.10) can be expressed in the following form :

$$\boldsymbol{KU} = \boldsymbol{F} \tag{3.11}$$

The fact that the displacements must be small has affected the calculations of $\boldsymbol{K}$ and $\boldsymbol{F}$ since integrations are performed in the initial element volume and the strain-displacement matrix $\boldsymbol{B}$ is independent of displacements while $\mathfrak{C}$ is constant.

3.2.2 Hyperelastic Solid Phase

As presented in Chapter 2 the stress state of the solid phase leads to large displacements and large strains while the material is defined by non-linear constitutive formulations. In such cases the deformation state is described either by Total or Upgraded Lagrangian description. Total Lagrangian (TL) description refers to all deformations with respect to the initial configuration, which is fixed in space while Updated Lagrangian (UL) description tracks material

points through the deformation process.

The aforementioned geometric and material non-linearities of the solid phase of the tissues impose a basic problem and that is to find the state of equilibrium of a body corresponding to the applied loads. This is achieved by an iterative procedure where the external load $\boldsymbol{F}$ is applied incrementaly between two successive time steps. Note that time-steps do not refer to the time domain rather than the pseudo time between two succesive applications of the incremental load.Suppose that the state of the system is known at time t and solution is seeken at $t+1$. Define the virtual displacement field $\delta^t u_i$ that are assumed to be the variation of the current displacement and correspond to the current Green-Lagrange ($\delta^t \epsilon_{ij}$) and small strain ($\delta^t e_{ij}$) tensors components[3]:

$$\delta\epsilon_{ij}^t = x_{m,i}^t x_{n,j}^t \delta e_{mn}^t \tag{3.12}$$

$$\delta e_{ij}^t = \frac{1}{2}\left(\frac{\partial \delta u_m}{\partial x_n^t} + \frac{\partial \delta u_n}{\partial x_m^t}\right) x_{m,i}^t x_{n,j}^t \delta e_{mn}^t \tag{3.13}$$

Equation (3.1) becomes:

$$\int_{V^0} S_{ij}^{t+1} \delta\epsilon_{ij}^{t+1} dV^0 = R^{t+1} \tag{3.14}$$

while by considering incremental decompositions it takes the following form:

$$\int_{V^t} S_{ij}^t \delta\epsilon_{ij}^t dV^t + \int_{V^t} \sigma_{ij}^t \delta\eta_{ij}^t dV^t = R^{t+1} - \int_{V^t} \sigma_{ij}^t \delta\epsilon_{ij}^t dV^t \tag{3.15}$$

with the incremental stress and strain tensors defined as follows:

$$S_{ij}^{t+1} = S_{ij}^t + S_{ij}^0 \tag{3.16}$$

$$\epsilon_{ij}^{t+1} = \epsilon_{ij}^t + \epsilon_{ij}^0 = \epsilon_{ij}^t + e_{ij}^0 + \eta_{ij}^0 = \frac{1}{2}(u_{i,j}^0 + u_{j,i}^0) + \frac{1}{2}(u_{k,i}^0 + u_{k,j}^0) r4 \tag{3.17}$$

By assuming that the second Piola-Kirchhoff stress tensor can be expressed as:

$$S_{ij}^0 = \int_{V^0} C_{ijrs} e_{rs}^0 dV^0 \tag{3.18}$$

while:

$$\delta\epsilon_{ij}^0 = \delta\epsilon_{ij}^0 \tag{3.19}$$

the equilibrium equation becomes:

$$\int_{V^0} C_{ijrs} e_{rs}^0 dV^0 + \int_{V^0} S_{ij}^t \delta\eta_{ij}^0 dV^0 = R^{t+1} - \int_{V^0} S_{ij} \delta e_{rs}^0 dV^0 \tag{3.20}$$

$$\boldsymbol{F}^{t+1} = \boldsymbol{F}^t + \boldsymbol{F} \tag{3.21}$$

$\boldsymbol{F}$ is the increment in nodal point forces correspondent to the increment in element displacements and stresses from t to $t+1$ and can be approximated using a tangent stiffness matrix $\boldsymbol{K}^t$ which corresponds to the geometric and material conditions at time t [3]:

$$\boldsymbol{F} = \boldsymbol{K}^t\boldsymbol{U} \tag{3.22}$$

where $\boldsymbol{U}$ is a vector of incremental nodal displacements so:

$$\boldsymbol{K} = \frac{\partial \boldsymbol{F}^t}{\partial \boldsymbol{U}^t} \tag{3.23}$$

It can be seen that:

$$\boldsymbol{K}^t\boldsymbol{U} = \boldsymbol{R}^{t+1} - \boldsymbol{F}^t \Rightarrow \boldsymbol{U}^{t+1} = \boldsymbol{U}^t + \boldsymbol{U} \tag{3.24}$$

By solving for $\boldsymbol{U}$ the displacements at $t+1$ are calculated as follows:

$$\boldsymbol{U}^{t+1} = \boldsymbol{U}^t + \boldsymbol{U} \tag{3.25}$$

The calculations are performed by implementing the widely used Newton-Raphson method that is an extension of the simple incremental technique. The Newton-Raphson algorithm, having calculated an increment in the nodal point displacements, which defines a new total displacement vector, repeats the incremental solution presented above using the currently known total displacements instead of the displacements at time t. For $i = 1, ...$ the Newton Raphson iteration is[3]:

$$\boldsymbol{K}^{t+1}_{(i-1)}\Delta\boldsymbol{U}^{(i)} = \boldsymbol{R}^{t+1} - \boldsymbol{F}^{t+1}_{(i-1)} \tag{3.26}$$

$$\boldsymbol{U}^{t+1}_{(i)} = \boldsymbol{R}^{t+1}_{(i-1)} + \Delta\boldsymbol{U}_{(i)} \tag{3.27}$$

with initial conditions:

$$\boldsymbol{U}^{t+1}_{(0)} = \boldsymbol{U}^t, \qquad \boldsymbol{K}^{t+1}_{(0)} = \boldsymbol{K}^t, \qquad \boldsymbol{F}^{t+1}_{(0)} = \boldsymbol{F}^t \tag{3.28}$$

More about the formulations in element base can be found in [3]

3.2.3 Convection-Diffusion-Production Equation

Consider the general form of the Convection Diffusion Equation :

$$\alpha(\boldsymbol{x})\frac{\partial \boldsymbol{\Phi}(\boldsymbol{x},t)}{\partial t} = \beta(\boldsymbol{x})\boldsymbol{\nabla}^2\boldsymbol{\Phi}(\boldsymbol{x},t) - \gamma(\boldsymbol{x})\nabla\cdot(\boldsymbol{v}\boldsymbol{\Phi}(\boldsymbol{x},t)) + \delta(\boldsymbol{x})\boldsymbol{\Phi}(\boldsymbol{x},t) + \epsilon(\boldsymbol{x}) \tag{3.29}$$

The physical space is discretized in N elements with M nodes each. We assume that the solution takes the form:

$$\boldsymbol{\Phi} \cong \boldsymbol{N\phi} = [N_1, ..., N_M] \begin{bmatrix} \phi_1 \\ \vdots \\ \phi_M \end{bmatrix} = N_i \phi_i \tag{3.30}$$

where N_i are the weight functions and ϕ_i are the nodal parameters.

$$\alpha \frac{\partial}{\partial t} \boldsymbol{N\phi} = \beta \boldsymbol{\nabla^2 N\phi} - \gamma \boldsymbol{v \nabla N\phi} + \delta \boldsymbol{N\phi} + \epsilon \tag{3.31}$$

Multiply with weight functions vector and integrate over the element volume:

$$\begin{aligned} \alpha \int_V \boldsymbol{N^T} \frac{\partial}{\partial t} \boldsymbol{N\phi} dV = \beta \int_V \boldsymbol{N^T \nabla^2 N\phi} dV - \gamma \boldsymbol{u} \int_V \boldsymbol{N^T} \nabla \boldsymbol{N\phi} dV \\ + \delta \int_V \boldsymbol{N^T N\phi} dV + \epsilon \int_V \boldsymbol{N^T} dV \end{aligned} \tag{3.32}$$

Nodal parameter ϕ_i is independent of space and time so by integrating by parts and ignoring the boundary integrals (3.32) can be written as:

$$\begin{aligned} \alpha \frac{\partial \boldsymbol{\phi}}{\partial t} \int_V \boldsymbol{N^T N} dV = -\beta \boldsymbol{\phi} \int_V \boldsymbol{\nabla}(\boldsymbol{N^T}) \boldsymbol{\nabla N} dV - \gamma \boldsymbol{v\phi} \int_V \boldsymbol{N^T \nabla N} dV \\ + \delta\phi \int_V \boldsymbol{N^T N\phi} dV + \epsilon \int_V \boldsymbol{N^T} dV \end{aligned} \tag{3.33}$$

(3.33) can be simplified to:

$$\boldsymbol{C\dot{\phi}} + \boldsymbol{K\phi} = \boldsymbol{F} \tag{3.34}$$

where:

$$\begin{aligned} \boldsymbol{K} &= \boldsymbol{X''} + \boldsymbol{X'} - \boldsymbol{X}, \\ \boldsymbol{C} &= \alpha \int_V \boldsymbol{N^T N}\, dV, & \boldsymbol{X'} &= \beta \int_V \boldsymbol{N^T \nabla N}\, dV, \\ \boldsymbol{X''} &= \gamma \int_V \boldsymbol{\nabla N^T \nabla N}\, dV, & \boldsymbol{X} &= \delta \int_V \boldsymbol{N^T N}\, dV, \\ \boldsymbol{F} &= \epsilon f \int_V \boldsymbol{N^T}\, dV \end{aligned}$$

3.3 Mesh

As previously mentioned, the computational domain portraying the TME comprises a quarter-sphere encased within a cube at the axis origin. Both the size and the characteristic length of the tumor domain mesh are significantly smaller compared to those of the host domain. This is attributed to the notorious heterogeneity between the two regions, where the intricate interactions within the tumor domain, as well as those occurring at the interface between the tumor and host domains, demand a higher resolution for precise modeling. By opting for a smaller domain size and a locally refined mesh for the tumor along with the adjacent area, a detailed portrayal of these interactions is achieved with significantly less computational resources.

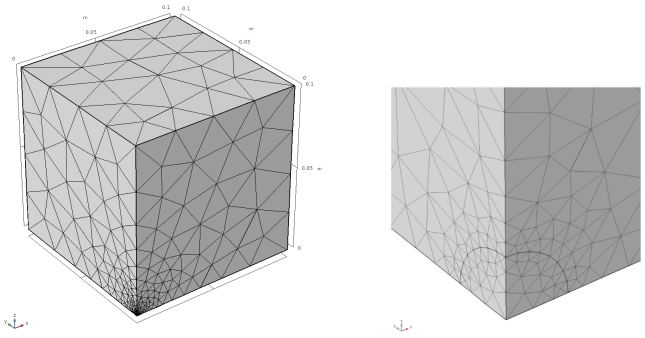

Figure 3.1: Mesh and zoom in tumor domain (change this!)

3.3.1 Finite Elements

The computational mesh is assembled with M tetrahedra finite elements e, with 4 nodes each and a single Gauss point in the center of mass as it can be seen in Figure 3.2.

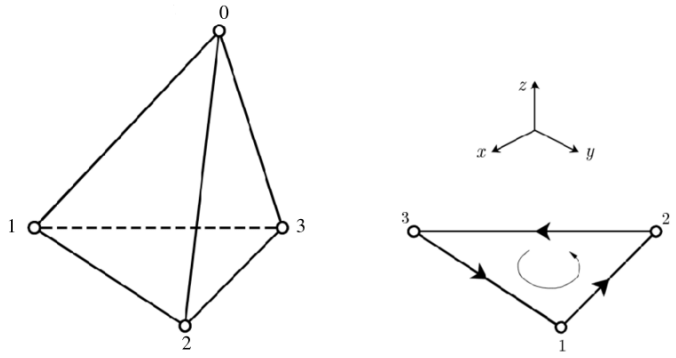

Figure 3.2: Tetrahedron element with four nodes in an orthonormal Cartesian coordinate system

A three dimensional vector field $\boldsymbol{\phi}(x, y, z)$ can be expressed at each node i as follows: [13]

$$\boldsymbol{\phi}_i(x, y, z) = \begin{Bmatrix} \boldsymbol{\phi}_{x,i}(x, y, z) \\ \boldsymbol{\phi}_{y,i}(x, y, z) \\ \boldsymbol{\phi}_{z,i}(x, y, z) \end{Bmatrix} \Rightarrow \boldsymbol{\phi}_i = \begin{Bmatrix} \boldsymbol{\phi}_{x,i} \\ \boldsymbol{\phi}_{y,i} \\ \boldsymbol{\phi}_{z,i} \end{Bmatrix}, i \in [0, 3] \tag{3.35}$$

The state of a vector field in a tetreahedron element is described by 12 degrees of freedom (DoF) and can be described in matrix form as follows:

$$\boldsymbol{\phi}^e = \begin{Bmatrix} \boldsymbol{\phi}_0 \\ \boldsymbol{\phi}_1 \\ \boldsymbol{\phi}_2 \\ \boldsymbol{\phi}_3 \end{Bmatrix} \tag{3.36}$$

The calculation of the unknown variables is achieved by a linear polynomial :

$$\phi(x, y, z) = a + bx + cy + dz \tag{3.37}$$

and for each degree of freedom with index $k \in [0, 11]$ the unknown values are expressed in matrix form as follows:

$$\boldsymbol{\phi}^e(x, y, z) = \begin{Bmatrix} \boldsymbol{\phi}_x(x, y, z) \\ \boldsymbol{\phi}_y(x, y, z) \\ \boldsymbol{\phi}_z(x, y, z) \end{Bmatrix} = \begin{bmatrix} 1\ x\ y\ z\ 0\ 0\ 0\ 0\ 0\ 0\ 0\ 0 \\ 0\ 0\ 0\ 0\ 1\ x\ y\ z\ 0\ 0\ 0\ 0 \\ 0\ 0\ 0\ 0\ 0\ 0\ 0\ 0\ 1\ x\ y\ z \end{bmatrix} \begin{Bmatrix} \alpha_0 \\ \vdots \\ \alpha_i \\ \vdots \\ \alpha_{11} \end{Bmatrix} = \boldsymbol{M}(x, y, z)\boldsymbol{\alpha} \tag{3.38}$$

Substitute the nodal coordinates in (3.38) and the expression for all the degrees of freedom of the element becomes:

$$\begin{Bmatrix} \phi_{x,0} \\ \phi_{y,0} \\ \phi_{z,0} \\ \vdots \\ \phi_{x,4} \\ \phi_{y,4} \\ \phi_{z,4} \end{Bmatrix} = \begin{bmatrix} 1\ x_1\ y_1\ z_1\ 0\ 0\ 0\ 0\ 0\ 0\ 0\ 0 \\ 0\ 0\ 0\ 0\ 1\ x_1\ y_1\ z_1\ 0\ 0\ 0\ 0 \\ 0\ 0\ 0\ 0\ 0\ 0\ 0\ 0\ 1\ x_1\ y_1\ z_1 \\ \cdots \\ 1\ x_4\ y_4\ z_4\ 0\ 0\ 0\ 0\ 0\ 0\ 0\ 0 \\ 0\ 0\ 0\ 0\ 1\ x_4\ y_4\ z_4\ 0\ 0\ 0\ 0 \\ 0\ 0\ 0\ 0\ 0\ 0\ 0\ 0\ 1\ x\ y_4\ z_4 \end{bmatrix} \begin{Bmatrix} \alpha_0 \\ \alpha_1 \\ \alpha_2 \\ \vdots \\ \alpha_9 \\ \alpha_{10} \\ \alpha_{11} \end{Bmatrix} \Rightarrow \boldsymbol{\phi}^e = \boldsymbol{A}\boldsymbol{\alpha} \tag{3.39}$$

Solve (3.39) and substitute $\boldsymbol{a}$ in (3.38) the shape functions N_i are obtained :

$$\boldsymbol{\phi} = \left\{ \begin{array}{c} \boldsymbol{\phi}_x \\ \boldsymbol{\phi}_y \\ \boldsymbol{\phi}_z \end{array} \right\} = \boldsymbol{M}\boldsymbol{A}^{-1}\boldsymbol{\phi}^e = \boldsymbol{N}\boldsymbol{\phi}^e = [\boldsymbol{N}_0, \boldsymbol{N}_1, \boldsymbol{N}_2, \boldsymbol{N}_3]\, \boldsymbol{\phi}^e \tag{3.40}$$

with:

$$\boldsymbol{N}_i = \begin{bmatrix} \boldsymbol{\nu_i} & 0 & 0 \\ 0 & \boldsymbol{\nu_i} & 0 \\ 0 & 0 & \boldsymbol{\nu_i} \end{bmatrix} = \boldsymbol{\nu}_i \boldsymbol{\delta_{ij}} \tag{3.41}$$

and

$$\nu_i = \frac{s_1 + b_1 x + c_1 y + d_1 z}{6V} \tag{3.42}$$

The coefficients for the components of the shape functions are calculated in a circular manner :

$$s_0 = \begin{vmatrix} x_1 & y_1 & z_1 \\ x_2 & y_2 & z_2 \\ x_3 & y_3 & z_3 \end{vmatrix}, \quad b_0 = -\begin{vmatrix} 1 & y_1 & z_1 \\ 1 & y_2 & z_2 \\ 1 & y_3 & z_3 \end{vmatrix}, \tag{3.43}$$

$$c_0 = \begin{vmatrix} x_1 & 1 & z_1 \\ x_2 & 1 & z_2 \\ x_3 & 1 & z_3 \end{vmatrix}, \quad d_0 = -\begin{vmatrix} x_1 & y_1 & 1 \\ x_2 & y_2 & 1 \\ x_3 & y_3 & 1 \end{vmatrix} \tag{3.44}$$

while the volume of the tetrahedral finite element is:

$$6V = \begin{vmatrix} 1 & x_0 & y_0 & z_0 \\ 1 & x_1 & y_1 & z_1 \\ 1 & x_2 & y_2 & z_2 \\ 1 & x_3 & y_3 & z_3 \end{vmatrix} \tag{3.45}$$

It is obvious that $\mathrm{tr}(\boldsymbol{N}) = 1$. For scalar fields the number of DoF for the element is reduced to 4. The manipulations in the above relations can be performed with ease.

Chapter 4

Discretization in the Time Domain

4.1 Introduction

In this section, the time integration schemes implemented for the transient analysis of the tumor micro-environment are presented. These methods are Backward Differentiation Formula, Newmark and Generalized-α. Each section contains the mathematical formulations as well as the corresponding algorithm for each integration method. The aforementioned methods are implemented in `MSolve` as Transient `IParentNumericalAnalyzers`. These analyzers are responsible for the orchestration of time-dependent finite element analyses, by managing time marching, creating data structures with respect to the methods coefficients and managing the state of the system. More information regarding `MSolve` Numerical Analyzers and their integration of into the simulation of the tumor micro-environment is provided in Chapter 5. Consider the equations of equilibrium governing the linear, transient response of a scalar or vector field $\boldsymbol{\phi}(\boldsymbol{x}, t)$:

$$\boldsymbol{M}\ddot{\boldsymbol{\phi}} + \boldsymbol{C}\dot{\boldsymbol{\phi}} + \boldsymbol{K}\boldsymbol{\phi} = \boldsymbol{F} \tag{4.1}$$

$\dot{\boldsymbol{\phi}}$ and $\ddot{\boldsymbol{\phi}}$ are the first and second temporal derivatives, respectively. $\boldsymbol{K}$, $\boldsymbol{C}$, $\boldsymbol{M}$ are the corresponding coefficient matrices defined by the constitutive properties of the medium corresponding to the second first and zeroth time derivative vectors. All methods presented are direct methods meaning that that they operate directly on (4.1) without transforming it. One core idea behind this methods is that instead of trying to satisfy (4.1) at any time t of the continuous time domain, they satisfy it at discrete time intervals Δt assuming local equilibrium. In addition to that all methods presented in this chapter are implicit, meaning that they make use of both current and previous time step information to advance the solution. This implicit nature allows for greater stability, especially for stiff equations

4.2 Newmark Integration Scheme

The Newmark-beta method is a numerical algorithm for solving second-order differential equations, commonly used in structural dynamics and other areas requiring the integration of motion equations. The method hinges on two key parameters, which are adjustable to control the numerical stability and accuracy of the integration. These parameters enable the method to be fine-tuned for conditional or unconditional stability, making it suitable for various applications. Its implicit nature allows for larger time steps than explicit methods, but this comes with increased computational demands due to the iterative solution of the resulting equations at each time step.

4.2.1 Mathematical Formulations

The Newmark integration method is based on the following assumptions for the calculation of the first and second derivatives of the solution [4], [26]:

$$\dot{\boldsymbol{\phi}}^{t+1} = \dot{\boldsymbol{\phi}}^{t} + \left[(1-\delta)\,\ddot{\boldsymbol{\phi}}^{t} + \delta\ddot{\boldsymbol{\phi}}^{t+1}\right]\Delta t \tag{4.2}$$

$$\boldsymbol{\phi}^{t+1} = \boldsymbol{\phi}^{t} + \dot{\boldsymbol{\phi}}^{t}\Delta t + \left[\left(\frac{1}{2}-\alpha\right)\ddot{\boldsymbol{\phi}}^{t} + \alpha\ddot{\boldsymbol{\phi}}^{t+1}\right]\Delta t^2 \tag{4.3}$$

where the superscripts t and $t+1$ denote the current and next time-step correspondingly while α and δ are determined to obtain the desired integration accuracy and stability. For $\alpha = 1/2$ and $\delta = 1/6$ the algorithm is called Linear Acceleration Method. For $\alpha = 1/2$ and $\delta = 1/4$, the algorithm is called Constant Average Acceleration Method (Trapezoidal Rule) and is unconditionally stable, meaning convergence is granted for any time-step.
Considering the trapezoidal rule, and solving for the primary variable at the next time increment $t+1$, Equation(4.1) becomes:

$$\left(\frac{4}{\Delta t^2}\boldsymbol{M} + \frac{2}{\Delta t}\boldsymbol{C} + \boldsymbol{K}\right)\boldsymbol{\phi}^{t+1} = \boldsymbol{R}^{t+1} + \boldsymbol{M}\left(\frac{4}{\Delta t^2}\boldsymbol{\phi^t} + \frac{4}{\Delta t}\dot{\boldsymbol{\phi}}^{\boldsymbol{t}} + \ddot{\boldsymbol{\phi}}^{\boldsymbol{t}}\right) + \boldsymbol{C}\left(\frac{2}{\Delta t}\boldsymbol{\phi^t} + \dot{\boldsymbol{\phi}}^{\boldsymbol{t}}\right) \tag{4.4}$$

The computations for the first and second derivatives at $t+1$ based on $\boldsymbol{\phi^{t+1}}$ are performed based on the Newmark integration coefficients presented in Table4.1:

4.2.2 Algorithm

The complete solution procedure using the Newmark method is summarized as follows:
A. Initial calculations:

a_0	$\dfrac{1}{\alpha \Delta t^2}$
a_1	$\dfrac{\delta}{\alpha \Delta t}$
a_2	$\dfrac{1}{\alpha \Delta t}$
a_3	$\dfrac{1}{2\alpha} - 1$
a_4	$\dfrac{\Delta t}{\alpha} - 1$
a_5	$\dfrac{\Delta t}{2}\left(\dfrac{\delta}{\alpha} - 2\right)$
a_6	$\Delta t(1-\delta)$
a_7	$\delta \Delta t$

Table 4.1: Newmark Method integration constants

1. Form matrices $\boldsymbol{M}^0$, $\boldsymbol{C}^0$, $\boldsymbol{K}^0$.
2. Initialize solution vector $\boldsymbol{\phi}^0$.
3. Select time step Δt and parameters α and δ. Calculate integration constants:

$$\delta \geq 0.5$$
$$\alpha \geq 0.25(0.5+\delta)^2$$

4. Calculate integration constants of Table(4.1)
5. Form effective matrix $\hat{\boldsymbol{K}}^0 = \boldsymbol{K}^0 + a_0\boldsymbol{M}^0 + a1\boldsymbol{C}^0$.

B. For each time step:

1. Form matrices $\boldsymbol{M}^t$, $\boldsymbol{C}^t$, $\boldsymbol{K}^t$. If the medium properties do not change over time skip this step.
2. Form effective matrix $\hat{\boldsymbol{K}}^t = \boldsymbol{K}^t + a_0\boldsymbol{M}^t + a1\boldsymbol{C}^t$. If the medium properties do not change over time skip this step.

3. Calculate effective RHS vector $\hat{\boldsymbol{R}}^{t+1}$ at time $t + \Delta t$.

$$\hat{\boldsymbol{R}}^{t+1} = \boldsymbol{R}^{t+1} + \boldsymbol{M}^t \left(a_0 \boldsymbol{\phi^t} + a_2 \dot{\boldsymbol{\phi}}^{\boldsymbol{t}} + a_3 \ddot{\boldsymbol{\phi}}^{\boldsymbol{t}} \right) + \boldsymbol{C}^t \left(a_1 \boldsymbol{\phi^t} + a_4 \dot{\boldsymbol{\phi}}^{\boldsymbol{t}} + a_5 \ddot{\boldsymbol{\phi}}^{\boldsymbol{t}} \right) + \boldsymbol{K}^t \alpha_f \phi^t \quad (4.5)$$

4. Solve $\hat{\boldsymbol{K}} \boldsymbol{\phi}^{t+1} = \hat{\boldsymbol{R}}^{t+1}$

5. Calculate the first and second derivatives at time $t + \Delta t$.

$$\ddot{\boldsymbol{\phi}}^{\boldsymbol{t+1}} = a_0 \left(\boldsymbol{\phi}^{t+1} - \boldsymbol{\phi}^t \right) - a_2 \dot{\boldsymbol{\phi}}^{\boldsymbol{t}} - a_3 \ddot{\boldsymbol{\phi}}^{\boldsymbol{t}}, \quad (4.6)$$

$$\dot{\boldsymbol{\phi}}^{\boldsymbol{t+1}} = \dot{\boldsymbol{\phi}}^{\boldsymbol{t}} + a_6 \ddot{\boldsymbol{\phi}}^{t} - a_7 \ddot{\boldsymbol{\phi}}^{\boldsymbol{t+1}}. \quad (4.7)$$

4.2.3 MSolve Implementation

4.3 Generalized - α Integration Scheme

The generalized-α integration scheme extends the Newmark Algorithm. It is a direct-time integration method that enhances stability by dissipating high-energy oscillations, often arising as numerical artifacts from discretization or approximations. In transient computational mechanics, these oscillations, not always inherent to the physical system, are effectively managed by selecting appropriate parameters, while preserving essential low-energy components.

4.3.1 Mathematical Formulations

The generalized-α method is based on the following assumptions [18], [11]:

$$\boldsymbol{\phi}^{t+1} = \boldsymbol{\phi}^t + \dot{\boldsymbol{\phi}}^t \Delta t + \left[\left(\frac{1}{2} - \beta \right) \Delta t^2 \boldsymbol{a}^t + \beta \Delta t^2 \boldsymbol{\alpha}^{t+1} \right] \quad (4.8)$$

$$\dot{\boldsymbol{\phi}}^{t+1} = \dot{\boldsymbol{\phi}}^t + \frac{1}{\Delta t} \left[(1 - \gamma) \Delta t^2 \boldsymbol{a}^t + \gamma \Delta t^2 \boldsymbol{\alpha}^{t+1} \right] \quad (4.9)$$

where β and γ are determined to obtain the desired integration accuracy and stability. The algorithm implements algorithmic accelerations, $\boldsymbol{\alpha}^t$, $\boldsymbol{\alpha}^{t+1}$, which are related to the actual accelerations of the system through the following recurrance relationship :

$$(1 - \alpha_m) \boldsymbol{a}^{t+1} + \alpha_m \boldsymbol{a}^t = (1 - \alpha_f) \ddot{\boldsymbol{\phi}}^{\boldsymbol{t+1}} + (\alpha_f) \ddot{\boldsymbol{\phi}}^{\boldsymbol{t}} \quad (4.10)$$

with α_m, α_f chosen to achieve the desirable stability and accuracy. Consider the spectral radius of the amplification matrix ρ_∞, as a function of the non-dimensional natural

period of the system: $\hat{\Delta}t = \Delta t/T$. The algorithm becomes unconditionally stable for $\rho_\infty = \rho(\Delta t \hat{\to} \infty) \in [0,1]$ where parameters α_m, α_f are selected as follows:

$$\alpha_m = \frac{2\rho_\infty}{\rho_\infty + 1} \tag{4.11}$$

$$\alpha_m = \frac{\rho_\infty}{\rho_\infty + 1} \tag{4.12}$$

If ρ_∞ vanishes for $\hat{\Delta}t \to \infty$, asymptotic annihilation is achieved and parameters γ, β are:

$$\gamma = \frac{1}{2} - \alpha_m + \alpha_f \tag{4.13}$$

$$\beta = \frac{1}{4}\left(1 - \alpha_m + \alpha_f\right)^2 \tag{4.14}$$

The integration constants of the Generalized-α method are presented in 4.2:

4.3.2 Algorithm

The algorithm for the Generalized-α can be summarized as follows:

A. Initial calculations:

1. Form matrices $\boldsymbol{M}^0$, $\boldsymbol{C}^0$, $\boldsymbol{K}^0$.
2. Initialize solution vector $\boldsymbol{\phi}^0$.
3. Select time step Δt, spectral radius ρ_∞ and calculate α_m, α_f.
4. If ρ_∞ vanishes calculate γ, β.
5. Calculate integration constants of Table(4.2)
6. Form effective matrix $\hat{\boldsymbol{K}}^0 = \boldsymbol{K}^0 + a_0\boldsymbol{M}^0 + a1\boldsymbol{C}^0$.

B. For each time step:

1. Form matrices $\boldsymbol{M}^t$, $\boldsymbol{C}^t$, $\boldsymbol{K}^t$. If the medium properties do not change over time skip this step.
2. Form effective matrix $\hat{\boldsymbol{K}}^t = +a_0\boldsymbol{M}^t + a1\boldsymbol{C}^t + (1-\alpha_f)\boldsymbol{K}^t$. If the medium properties do not change over time skip this step.
3. Calculate effective RHS vector $\hat{\boldsymbol{R}}^{t+1}$ at time $t + \Delta t$.

$$\hat{\boldsymbol{R}}^{t+1} = \boldsymbol{R}^{t+1} + \boldsymbol{M}^t\left(a_0\boldsymbol{\phi^t} + a_0\dot{\boldsymbol{\phi}}^{\boldsymbol{t}} + a_3\ddot{\boldsymbol{\phi}}^{\boldsymbol{t}}\right) + \boldsymbol{C}^t\left(a_0\boldsymbol{\phi^t} + a_4\dot{\boldsymbol{\phi}}^{\boldsymbol{t}} + a_5\ddot{\boldsymbol{\phi}}^{\boldsymbol{t}}\right) + \boldsymbol{K}^t\alpha_f\boldsymbol{\phi}^t \tag{4.15}$$

a_0	$\frac{1-\alpha_m}{\beta\Delta t^2}$
a_1	$\frac{\gamma(1-\alpha_f)}{\beta\Delta t}$
a_2	$\frac{1-\alpha_m}{\beta\Delta t}$
a_3	$\frac{1-\alpha_m-2\beta}{2\beta}$
a_4	$\frac{\gamma-\gamma\alpha_f-\beta}{\beta}$
a_5	$\frac{(\gamma-2\beta)(1-\alpha_f)\Delta t}{2\beta}$
a_6	$\frac{\gamma}{\beta\Delta t}$
a_7	$\frac{\gamma-\beta}{\beta}$
a_8	$\frac{(\gamma-2\beta)\Delta t}{2\beta}$
a_9	$\frac{1}{\beta\Delta t^2}$
a_{10}	$\frac{1}{\beta\Delta t}$
a_{11}	$\frac{1-2\beta}{2\beta}$

Table 4.2: Generalized-α Method integration constants

4. Solve $\hat{\boldsymbol{K}}\boldsymbol{\phi}^{t+1} = \hat{\boldsymbol{R}}^{t+1}$

5. Calculate the first and second derivatives at time $t + \Delta t$.

$$\dot{\boldsymbol{\phi}}^{\boldsymbol{t+1}} = a_6\left(\boldsymbol{\phi}^{t+1} - a_7\dot{\boldsymbol{\phi}}^{t} - a_8\ddot{\boldsymbol{\phi}}^{\boldsymbol{t}}\right) \tag{4.16}$$

$$\ddot{\boldsymbol{\phi}}^{\boldsymbol{t+1}} = a_9\left(\boldsymbol{\phi}^{t+1} - a_{10}\dot{\boldsymbol{\phi}}^{t} - a_{11}\ddot{\boldsymbol{\phi}}^{\boldsymbol{t}}\right) \tag{4.17}$$

$$\tag{4.18}$$

4.4 Backward Differentiation Formula Time Integration Scheme

The Backward Differentiation Formula (BDF) method is a widely used numerical technique for solving stiff ordinary differential equations (ODEs) and partial differential equations (PDEs) in transient simulations. Belonging to the category of linear multistep methods, BDF approximates derivatives by employing implicit differentiation formulas and integrates equations over specified time intervals. Mathematically, the method constructs a linear combination of current and previous solutions to predict future values, with the precision of approximations being dependent on the step size. Noteworthy for its numerical stability, especially in the context of stiff equations, BDF also possesses the capability to accommodate variable time-stepping, a feature that is especially advantageous in scenarios where the solution experiences rapid transitions. This method, substantiated by its mathematical robustness, finds extensive application across various scientific and engineering domains, illustrating its crucial role in facilitating accurate and efficient numerical simulations in temporal analyses. In the scope of this thesis, the BDF method is implemented for solving first-order ordinary differential equations (ODEs) with a consistent timestep.

4.4.1 Mathematical Formulations

BDF is classified as an implicit method meaning it determines the system's state at a current time, denoted $\Phi(t^{n+N})$, by utilizing both the current and preceding time states, $\Phi(t^{n-(N-1)})$, $\ldots$, $\Phi(t^n)$, where N signifies the maximum number of previous time states involved in the calculations. Enhancing the numerical scheme by reducing the cut-off error becomes possible by increasing the count of considered previous states (N). The numerical schemes are deduced by evaluating Taylor's series expansions around $\Phi(t^{n+\lambda})$ as expressed below:

$$\sum_{n=0}^{\inf} \frac{\Phi^{(k)}(t^{n+\lambda})}{k!}\Delta t^n = \Phi(t^{n+\lambda}) - \frac{\partial\Phi(t^{n+\lambda})}{\partial t}\Delta t + \frac{\partial^2\Phi(t^{n+\lambda})}{\partial t^2}\Delta t^2 + O(\Delta t^3)$$

where $\lambda = 1...N$ is the number of previous time states, k is the order of the derivative, which for our case is 1 or 2 and $\Delta t = t^{n+\lambda} - t^n$. After some routine mathematical manipulation the expressions for the first backward derivative ($N = 5$) are :

$$\frac{\partial\Phi}{\partial t} = \frac{\Phi^{n+1} - \Phi^n}{\Delta t} + O(\Delta t) \tag{4.19}$$

$$\frac{\partial\Phi}{\partial t} = \frac{3\Phi^{n+2} - 4\Phi^{n+1} + \Phi^n}{2\Delta t} + O(\Delta t^2) \tag{4.20}$$

$$\frac{\partial \Phi}{\partial t} = \frac{11\Phi^{n+3} - 18\Phi^{n+2} + 9\Phi^{n+1} - 2\Phi^{n}}{6\Delta t} + O(\Delta t^3) \tag{4.21}$$

$$\frac{\partial \Phi}{\partial t} = \frac{25\Phi^{n+4} - 48\Phi^{n+3} + 36\Phi^{n+2} - 16\Phi^{n+1} + 3\Phi^{n}}{12\Delta t} + O(\Delta t^4) \tag{4.22}$$

$$\frac{\partial \Phi}{\partial t} = \frac{137\Phi^{n+5} - 300\Phi^{n+4} + 30\Phi^{n+3} - 200\Phi^{n+2} + 75\Phi^{n+1} + 12\Phi^{n}}{60\Delta t} + O(\Delta t^5) \tag{4.23}$$

Since the second derivative terms are not considered in this scheme ($\boldsymbol{M} = \boldsymbol{0}$) equation (4.1) takes the form :

$$\boldsymbol{C}\dot{\boldsymbol{\phi}} + \boldsymbol{K}\boldsymbol{\phi} = \boldsymbol{F} \tag{4.24}$$

The genreral form of the numerical scheme takes the form:

$$\boldsymbol{C}\frac{c_N\boldsymbol{\phi}^{n+N} + ... + c_1\boldsymbol{\phi}^{\boldsymbol{n}}}{c_t\Delta t} + \boldsymbol{K}\boldsymbol{\phi}^{n+1} = \boldsymbol{F} \Rightarrow$$

$$\left(\frac{c_N}{c_t\Delta t}\boldsymbol{C} + \boldsymbol{K}\right)\boldsymbol{\phi}^{n+N} = \boldsymbol{F} + \frac{1}{\Delta t}\boldsymbol{C}\left(-\frac{c_{n+N-1}}{c_t}\boldsymbol{\phi}^{n+N-1} ... - \frac{c_n}{c_t}\boldsymbol{\phi}^{n}\right) \Rightarrow$$

$$\hat{\boldsymbol{K}}^{(N)}\boldsymbol{\phi}^{n+N} = \hat{\boldsymbol{R}}^{(N)} \tag{4.25}$$

BDF 1 (N=1)

$$\hat{\boldsymbol{K}^{(1)}} = \frac{1}{\Delta t}\boldsymbol{C} + \boldsymbol{K}$$

$$\hat{\boldsymbol{R}^{(1)}} = \boldsymbol{F} + \frac{1}{\Delta t}\boldsymbol{C}\boldsymbol{\phi}^{n}$$

BDF 2 (N=2)

$$\hat{\boldsymbol{K}^{(2)}} = \frac{3}{2\Delta t}\boldsymbol{C} + \boldsymbol{K}$$

$$\hat{\boldsymbol{R}^{(2)}} = \boldsymbol{F} + \frac{1}{\Delta t}\boldsymbol{C}\left(\frac{4}{2}\boldsymbol{\phi}^{n+1} - \frac{1}{2}\boldsymbol{\phi}^{n}\right)$$

BDF 3 (N=3)

$$\hat{\boldsymbol{K}^{(3)}} = \frac{11}{6\Delta t}\boldsymbol{C} + \boldsymbol{K}$$

$$\hat{\boldsymbol{R}^{(3)}} = \boldsymbol{F} + \frac{1}{\Delta t}\boldsymbol{C}\left(\frac{18}{6}\boldsymbol{\phi}^{n+2} - \frac{9}{6}\boldsymbol{\phi}^{n+1} + \frac{2}{6}\boldsymbol{\phi}^{n}\right)$$

BDF 4 (N=4)

$$\hat{\boldsymbol{K}}^{(4)} = \frac{25}{12\Delta t}\boldsymbol{C} + \boldsymbol{K}$$

$$\hat{\boldsymbol{R}}^{(4)} = \boldsymbol{F} + \frac{1}{\Delta t}\boldsymbol{C}\left(\frac{48}{12}\boldsymbol{\phi}^{n+3} - \frac{36}{12}\boldsymbol{\phi}^{n+2} - \frac{16}{12}\boldsymbol{\phi}^{n+1} - \frac{3}{12}\boldsymbol{\phi}^{n}\right)$$

BDF 5 (N=5)

$$\hat{\boldsymbol{K}}^{(5)} = \frac{137}{60\Delta t}\boldsymbol{C} + \boldsymbol{K}$$

$$\hat{\boldsymbol{R}}^{(5)} = \boldsymbol{F} + \frac{1}{\Delta t}\boldsymbol{C}\left(\frac{300}{60}\boldsymbol{\phi}^{n+4} - \frac{300}{60}\boldsymbol{\phi}^{n+3} + \frac{200}{60}\boldsymbol{\phi}^{n+2} - \frac{75}{60}\boldsymbol{\phi}^{n+1} + \frac{12}{60}\boldsymbol{\phi}^{n}\right)$$

4.4.2 Algorithm

The complete solution procedure using the Backward Differentiation Formula method is summarized as follows:

A. Initial calculations:

1. Form matrices $\boldsymbol{C}^0$, $\boldsymbol{K}^0$.
2. Initialize solution vector $\boldsymbol{\phi}^0$.
3. Select time step Δt and method order $N = 1...5$
4. Form $\hat{\boldsymbol{K}}^1$ $\hat{\boldsymbol{F}}^1$. If there is no special treatment for the initial step the cut-off error will be of order 1 and the solution will be based on the initial value.

B. For each time step:

1. Form matrices $\boldsymbol{C}^t$, $\boldsymbol{K}^t$.
2. Form $\hat{\boldsymbol{K}}^N$ $\hat{\boldsymbol{F}}^N$. If the current step index i^t is smaller than the method order N then select the BDF$^{(i^t)}$
3. Solve $\hat{\boldsymbol{K}}^N \boldsymbol{\phi}^{t+1} = \hat{\boldsymbol{R}}^N$
4. Calculate derivative $\dot{\boldsymbol{\phi}}^{t+1}$ if needed.

Chapter 5

Solution Strategy

5.1 Intoduction

The coupled system of equations described in the preceding chapters is numerically solved using the Bio-mechanics module of MSolve. For validation, results are compared against those from COMSOL to ensure the robustness and accuracy of the implemented solution strategy. The challenges presented by the coupling of these equations necessitate a meticulous and adaptable approach.

Central to this strategy is a modular setup. Each partial differential equation, representing distinct physical phenomena, is formulated independently. Once these individual models are delineated, they are systematically integrated into a cohesive coupling framework, ensuring the interactions and dependencies between them are adequately addressed.

Given the inherent coupling between the equations, a staggered methodology is adopted for the solution. In this approach, equations are solved sequentially within each time step. This process is repeated iteratively until convergence criteria are met for all equations within the time-step. Following this, shared properties are updated and the simulation advances to the next time-step, and the iterative process is initiated once more.

This design choice empowers users with extensive flexibility in manipulating model parameters and coupling mechanisms. Users can isolate the one-way or two-way communication between equations and prescribe the shared properties to specific values. Additionally, the analysis can be finely tuned by adjusting the tolerances of each iterative process and by choosing from a variety of solvers and time integration methods.

5.2 Finite Elements Models Setup and Coupling

The framework offers a streamlined, templated format for creating distinct finite element models for any combination of the five equations described in Chapter 3, while it simplifies the integration of more equations. Each provider class is responsible for setting up the essential components needed to solve a specific equation. The core utilities of these classes can be summarized in the following paragraphs.

Initially model providers initialize the finite element model of the corresponding equation based on the input mesh, boudary and initial conditions. Appropriate field and material properties are assigned to each element, considering any possible coupled quantities from other equations of the system. Another basic task of the equation model provider is to set up the appropriate numerical solver, parent (transient) and child (equilibrium) analyzers, ensuring that the model is solved implementing the most suitable numerical methods. Additionally model providers perform the necessary calculations of the derivative quantities calculated at the Gauss points of each elements by leveraging the isoparametric interpolations and quadrature techniques, a pivotal step since these values often serve as shared quantities between equations. Last but not least providers are responsible for logging by facilitating the storage of values for the monitored degrees of freedom.

The coupled model provider orchestrates the integration and synchronization of the aforementioned equation model providers within the analysis. It plays a major role in initializing models, managing boundary conditions, updating shared quantities, and ensuring consistent advancements across all models at each simulation time step. Additionally, it handles the initialization and updating of analyzers and solvers, facilitates state saving, and updates time parameters, ensuring a harmonious and efficient simulation progression.

5.3 MSolve Analyzers

5.3.1 Transient (Parent) Analyzers

MSolve `IParentAnalyzer`, in the case of tumor modeling facilitate the management and coordination of transient analyses, acting as a hierarchical overseer to child analyzers. By establishing a hierarchical structure, parent analyzers ensure the integration of specialized child analyzers, each addressing distinct aspects of simulations. Parent analyzers manage the evolving state of simulations and provide mechanisms for creating linear algebra data structures, tracking progress, updating and storing states between steps. The construction of a parent analyzer involves initializing the algorithm and setting up the physical model, time pa-

rameters, and any additional method-specific parameters. For example, in algorithms of the Newmark family, this would include calculating integration constants that are subsequently used in various steps of the algorithm. The parent analyzer is responsible for constructing the effective system matrices, incorporating contributions from various coefficient matrices each scaled by the integration specific constants. Furthermore, parent analyzers manage the computation of the effective right-hand side (RHS) vectors, integrating contributions, external forces and internal force vectors derived from initial conditions and computed solutions of the primary variables and their derivatives. This ensures the maintenance of system equilibrium at each time step.

By establishing a clear hierarchy and delineating responsibilities, parent analyzers in MSolve bring order and efficiency to complex simulations, ensuring that each component of the system is addressed appropriately and that the overall solution is achieved in a systematic and reliable manner.

5.3.2 Staggered Analyzer

The `StepwiseStaggeredAnalyzer` class in MSolve is employed for addressing coupled problems through a staggered, iterative approach. This analyzer introduces functionalities to ensure seamless integration with analyzers that operate on a per-step basis, accommodating an array of nested parent analyzers each assigned with the manipulation for handling and solving specific equations of the coupled system. It orchestrates the step-by-step analysis, iteratively invoking each nested analyzer to solve its respective part of the problem for the current step before proceeding to the next. This ensures that interactions between different physical phenomena are captured and iteratively adjusted until the solution converges or the maximum number of staggered steps is reached, catering to both steady-state and transient systems.

The computational process is summarized as follows: At the beginning of each time step or set of staggered steps, all shared properties are communicated, with communications blocked until the beginning of the subsequent step. The staggered analyzer then sequentially calls the parent analyzers to solve the corresponding equations, calculates the norm between two successive solutions, and iteratively performs the process until convergence is achieved or the maximum iteration limit is reached. Upon convergence, the solution advances to the next temporal increment.

Inheriting state management and error tracking capabilities from `StaggeredAnalyzerBase`, the `StepwiseStaggeredAnalyzer` builds upon this foundation to perform necessary state updates, error computations, and convergence checks accurately, maintaining a record of

current solutions and corrections at each staggered step to facilitate error computation and assess convergence.

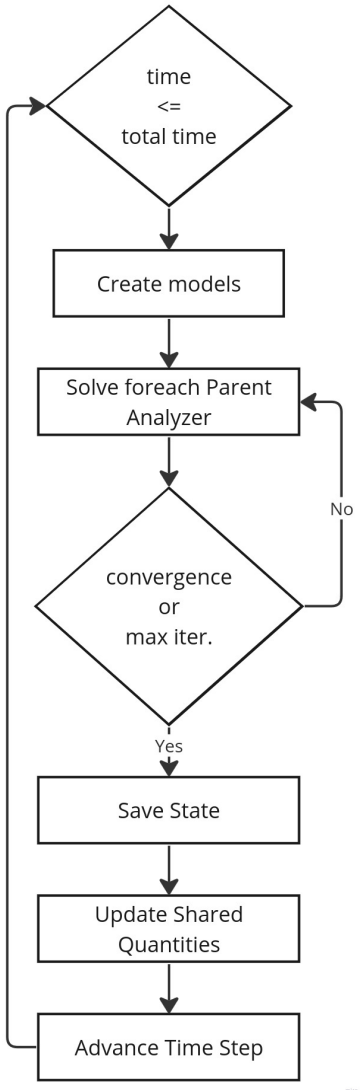

Figure 5.1: Step-wise Transient Analysis Flow Chart.

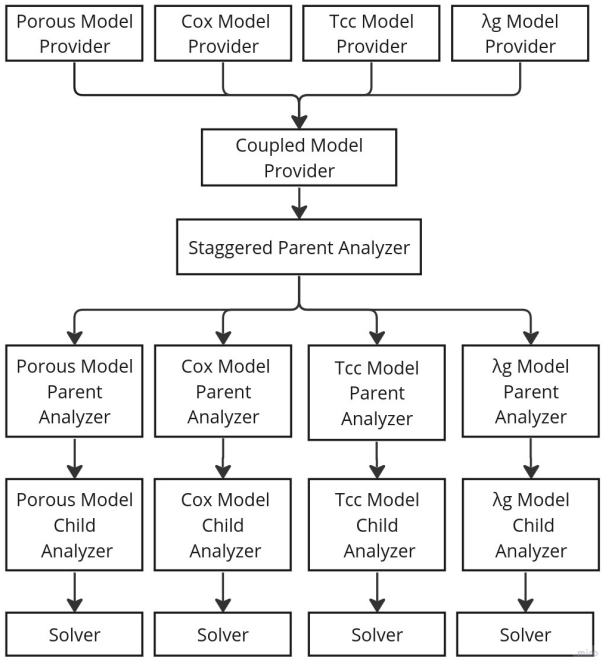

Figure 5.2: Coupled Finite Element Setup In Msolve.

5.3.3 Equilibrium (Child) Analyzers

The `IChildAnalyzer` interface provides the foundational blueprint for the analysis. It is designed to grapple linear as well as non-linear problems where equilibrium is assumed. They are operated and initialized by the parent analyzer and by providing Linear algebra intricacies, combined with the specific mechanics of the problem, they necessitate the appropriate

procedures to achieve an accurate solution. Every `IChildAnalyzer` utilizes the assigned `ISolver` to perform the numerical solution and provide the corresponding solution vector.

5.3.3.1 Load Control Analyzer

The `LoadControlAnalyzer` MSolve class adopts a load control strategy tailored to address the complexities of material and geometric non-linearities. The external load is applied incrementally, breaking down the problem into smaller, more manageable segments and allowing for a detailed evaluation of the system's response at each stage. This methodical approach aids in navigating through the non-linearities, aiming to enhance the stability and reliability of the solution process.

The design of the LoadControlAnalyzer encompasses several key functionalities. The incremental loading feature ensures that the external load is divided into well-defined increments, facilitating a step-by-step adjustment of the system's state vector, which encapsulates primary variables such as displacements. These adjustments are closely tied to linear algebraic operations, ensuring a level of precision necessary for iterative refinement.

In managing the iterations within each load increment, the class plays a pivotal role in ensuring that the computational process is efficient and accurate. It oversees the coordination of linear algebra operations, including matrix manipulations and solutions to linear systems, and ensures that the iterative process is kept within prescribed limits. In scenarios where convergence is not attained within these limits, the class has the capability to halt the analysis, prompting a reassessment of the situation.

Furthermore, the class is responsible for updating the system's state once convergence is achieved for a particular load increment. This involves refreshing not just the primary variables, such as displacements, but also derived quantities like strains and stresses, ensuring that all aspects of the system are accurately represented and up to date.

In summary, the LoadControlAnalyzer provides a structured and incremental approach to handling nonlinearities in material and geometric aspects of the problem. Through its careful management of load increments, iterative processes, and state updates, it aims to deliver a stable and reliable solution, contributing to the overall robustness of MSolve

5.3.3.2 Linear Analyzer

The Linear `IChildAnalyzer` is responsible for the treatment of linear mechanical systems in equilibrium. It is utilized by the parent analyzer to solve the system of equations derived

by the considered equilibrium state between two successive time-steps, or in the context of a steady state analysis.

5.4 Solver

`ISolver` is an MSolve interface that lies in the heart of every computational analysis. MSolve has a plethora of direct, point and stationary iterative solvers implemented each designed to tackle the specific needs of the problem with efficiency and accuracy. Child Analyzers provide solvers with the linear system representing the physical problem and the latter proceed to the solution. In the context of this research all matrices are non-symmetric due to the convection terms at Equations 2.27, 2.26, 2.28 or the non-symmetric nature of the mololithic coupling of Equations 2.16, 2.4. As a result all linear systems are solved with the LU solver of SuiteSparse for C#.

Chapter 6

Numerical Application and Results

6.1 Applications Description

In this chapter the results of the computational analyses performed are presented. The mathematical model consists of four partial and one ordinary differential equations and aims to simulate the tumor microenvironment by considering the interactions between cancer cells and oxygen tranpsort phenomena and the stress state due the tumor growth and the hydrostatic pressure of the interstitial fluid flow. By designing and implementing the proper Analyzers and data structures of the MSolve framework, as shown in Chapter 5, the coupled system of transient differential equations presented in Chapter2 are properly discretized in the space and time domains as shown in Chapter3 and solved in a seggregated way for the examined time period.

The stress flows in the porous tissues due to the interstitial fluid pressure (2.4) and the stresses of the solid matrix (2.16) are treated and solved as a single equation while O_2 concentration in the host region (2.27), the population of cancer cells (2.28) as well as the growth stretch ratio (2.24) are described by a linear convection-diffusion-reaction equation. O_2 concentration in the tumor region (2.26) is modeled with a convection-diffusion-reaction equtaion with a non-linear source term. The response of the solid phase is examined under two different constitutive laws. One that allows small strains and the influence of the growth in the strain field is neglected and a second where the tissues are considered as hyperelastic with large displacements, large strains and non-linear stress-strain relation with tumor growth influence included in the deformation gradient tensor. Healty and tumor regions are notoriously heterogenous. The aformentioned heterogenity is captured by varying model coefficients and equation forms across the two domains. Clinical data has shown that tumor tissues are orders of magnitude stiffer than healthy tissues while the same pattern can be seen in the hydraylic conductivity. This leads to significantly different stress states hence signifficantly different

TME responses. All model coefficients are presented in Table 6.1.

Parameter	**Tumor Value**	**Host Value**	**Units**
μ	22.44	5	kPa
k	216.7	6.667	kPa
k_{th}	7.52E-11	7.52E-13	m^2/kPa·s
S_v	7E3	7E3	m^{-1}
c_{iox}	0.2	0.2	mol/m^3
D_{ox}	1.79E-9	1.79E-9	m^3/s
P_{er}	3.55E-4	3.55E-4	m/s
A_{ox}	2.55E-2	-	mol/m^3s
k_{ox}	4.64E-3	-	mol/m^3
k_1	1.74E-6	-	1/s
k_2	8.3E-3	-	mol/m^3
p_v	4	4	kPa
p_l	0	0	kPa
L_p	2.794E-9	2.794E-9	m^2/kPa·s
$L_{pl}S_{vl}$	3.75E-1	3.75E-1	1/kPa·s

Table 6.1: Model Parameters

The computational domain consists of two regions. The tumor region is represented by an eighth of a sphere with radious $r = 5E-4[m]$ embeded in an eighth of a cube with edge $a = 0.1[m]$ representing the host tissue. The domain is discretized with 733 nodes and 2815 linear tetrahedra elements each with one Gauss Point positioned in the elemental center of mass. The mesh inside and close to the tumor regions are significantly more refined since all the phenomena of interest take place there. All spatial discretization parameters are shown in Table 6.2.

Domain Edge Size	1E-1 [m]
Initial Tumor Radius	5E-4 [m]
Nodes	733
Elements	2815
Nodes	733
Gauss Points / Element	1
Element Type	Tetrahedron

Table 6.2: Discrete Computational Domain Parameters

The computational solution has been performed using the Bio-Mechanics module of MSolve,

and the results are validated with COMSOL. To simulate a complex, multi-physics model such as that of the TME, our team at MGroup is actively developing and validating a new Bio-Mechanics sub-module for MSolve. The development process includes integrating and benchmarking new Convection-Diffusion-Reaction finite elements, hyper-elastic material constitutive laws, BDF, and Generalized-α transient analyzers, as well as the staggered step-wise analyzer. The analysis process can be summarized as follows: Each equation of the coupled system is represented by a model provider, and the corresponding transient response at each time-step is calculated by a pair of case-specific child and parent analyzers. The coupling between the equations, in terms of shared property communication, is performed by the coupled model provider. Meanwhile, the coupled solution at each time-step is achieved by the staggered analyzer, which orchestrates the analyzers, and each equation is solved iteratively until convergence is achieved.

Equation	**Parent Analyzer**	**Child Analyzer**	**Solver**
$\boldsymbol{u}$, p_i	Generalized-α	Load Control	Dense LU
c_{ox}	Generalized-α	Load Control	Dense LU
T_{cc}	Generalized-α	Linear	Dense LU
λ_g	Generalized-α	Linear	Dense LU

Table 6.3: Msolve Analysis components

Total Time	30 [d]
Step Size	3600 [s]
Total Steps	720

Table 6.4: Time Discretization Parameters for linear and elastic material analysis

Total Time	3 [d]
Step Size	variable [s]
Total Steps	448

Table 6.5: Time Discretization Parameters for hyperelastic material analysis

6.2 Numerical Results - Linear & Elastic Material

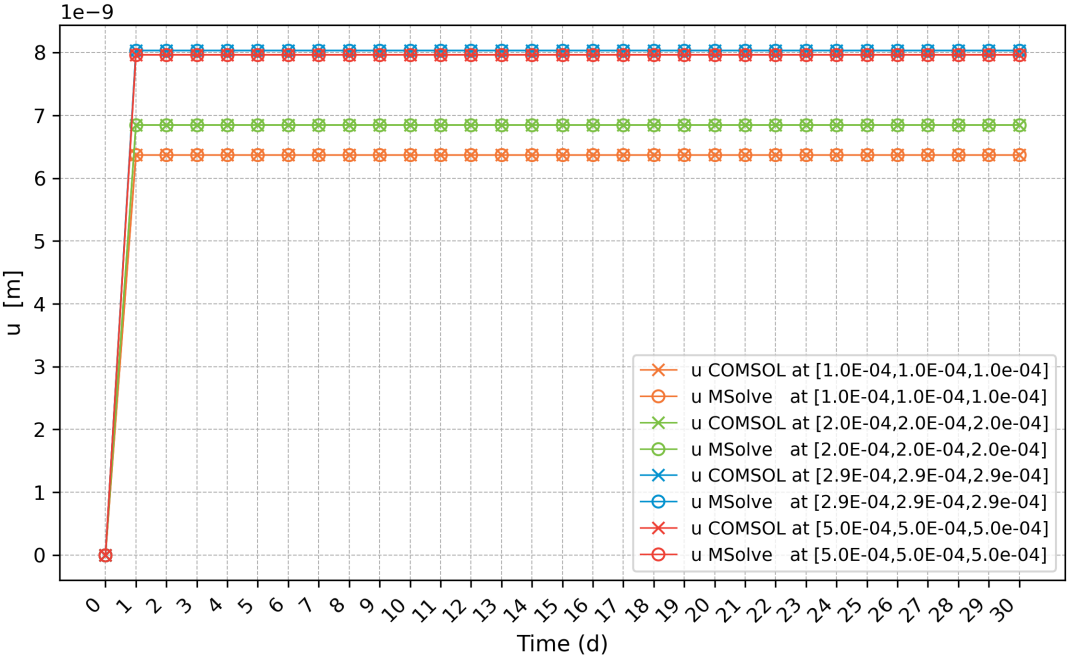

Figure 6.1: Solid Phase Displacement in x-direction over time at the specified nodal coordinates for linear and elastic solid phase tissues.

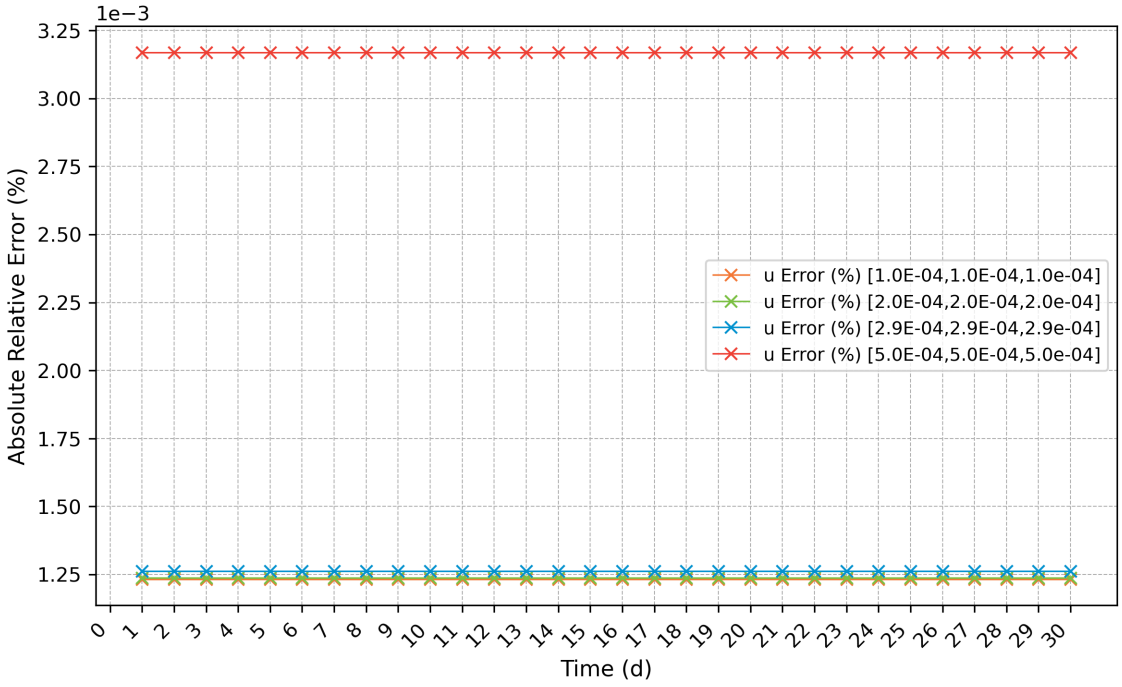

Figure 6.2: Absolute Relative Error (%) of the Solid Phase Displacement in x-direction over time at the specified nodal coordinates for linear and elastic solid phase tissues.

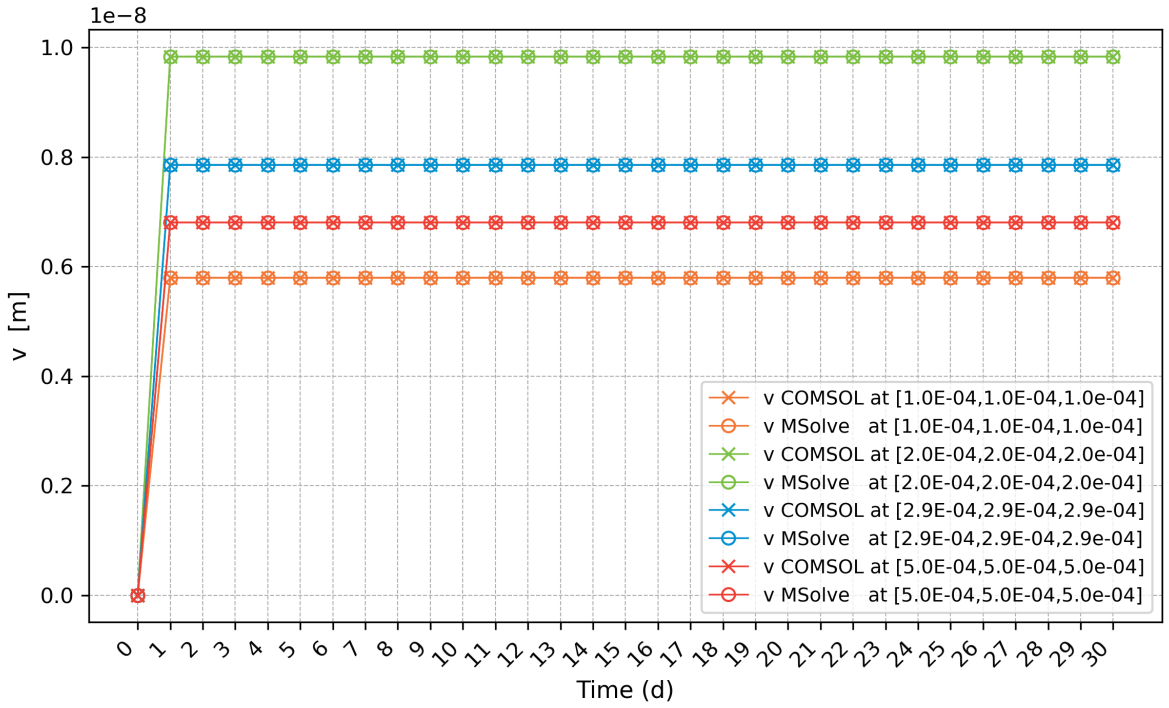

Figure 6.3: Solid Phase Displacement in y-direction over time at the specified nodal coordinates for linear and elastic solid phase tissues.

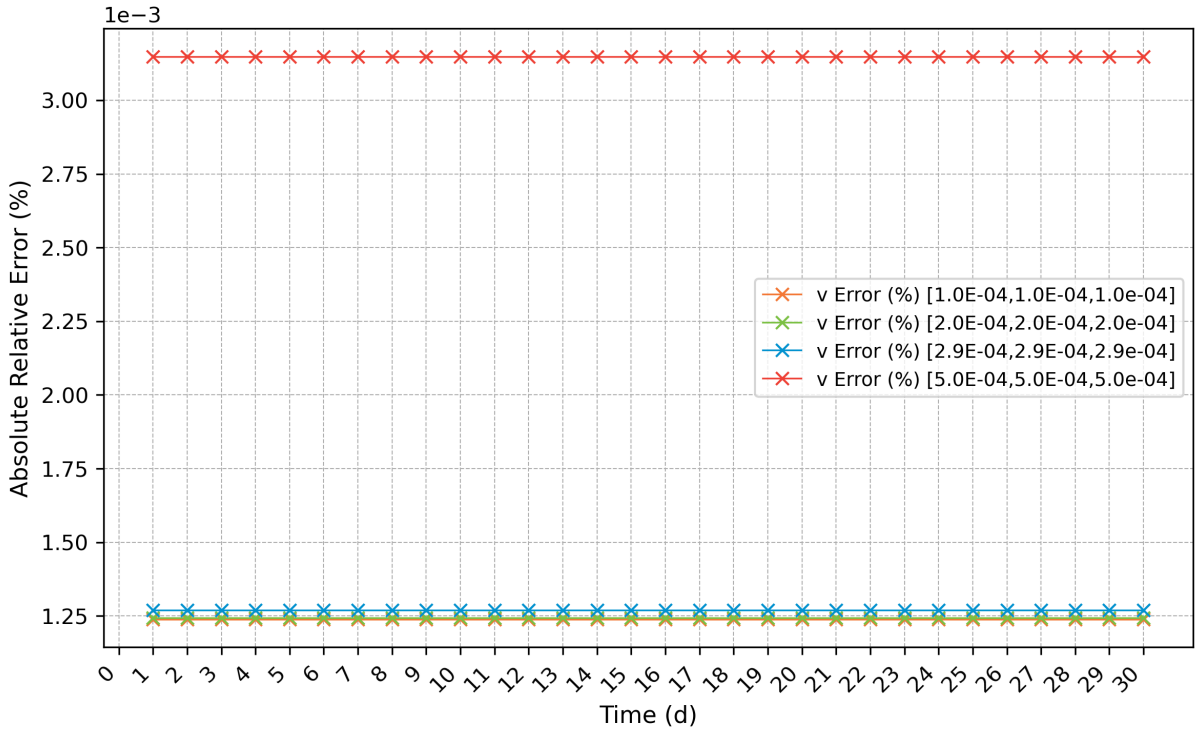

Figure 6.4: Absolute Relative Error (%) of the Solid Phase Displacement in y-direction over time at the specified nodal coordinates for linear and elastic solid phase tissues.

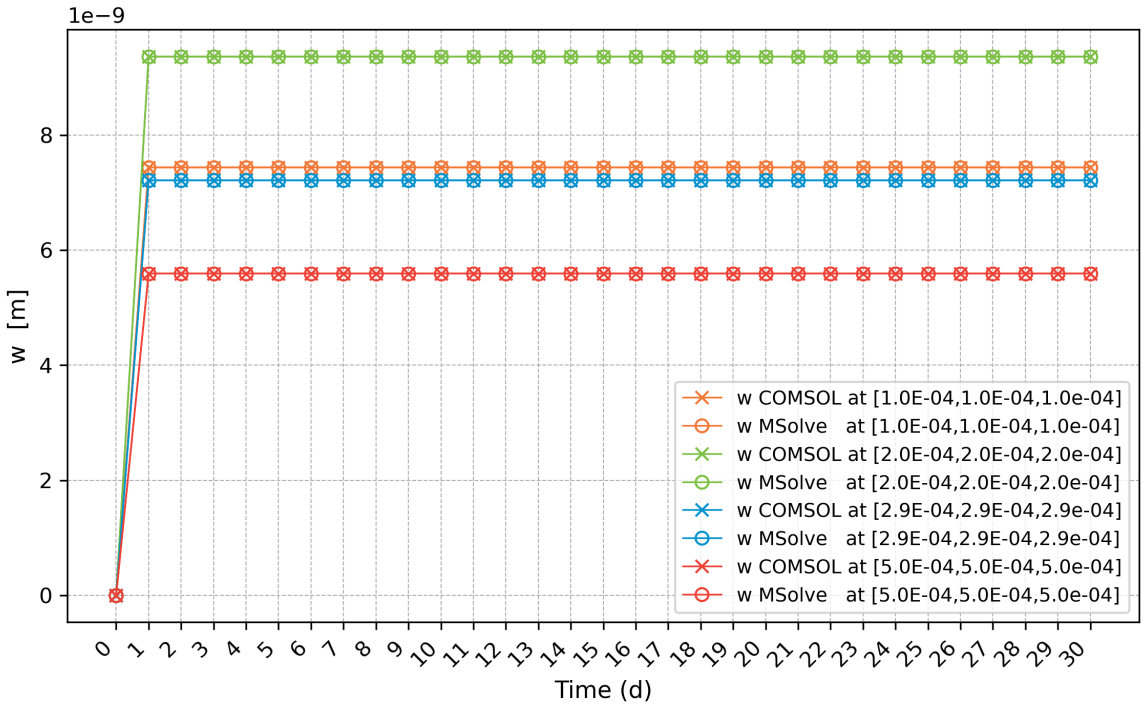

Figure 6.5: Solid Phase Displacement in z-direction over time at the specified nodal coordinates for linear and elastic solid phase tissues.

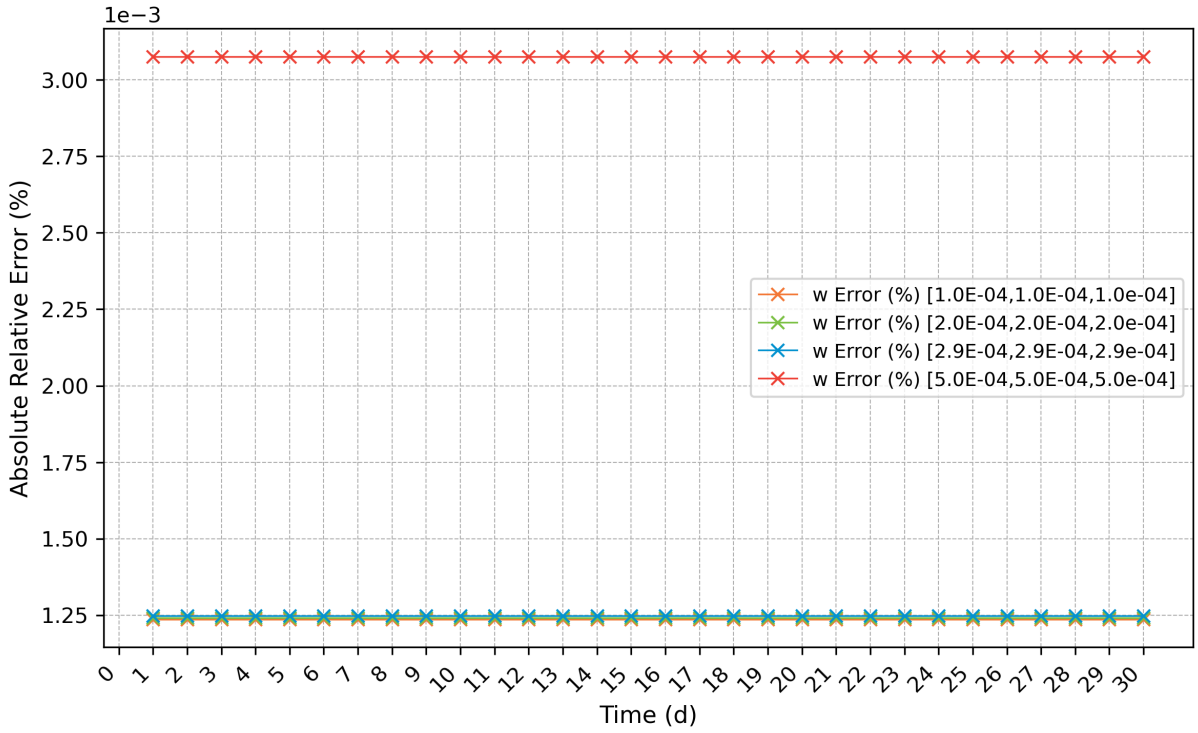

Figure 6.6: Absolute Relative Error (%) of the Solid Phase Displacement in z-direction over time at the specified nodal coordinates for linear and elastic solid phase tissues.

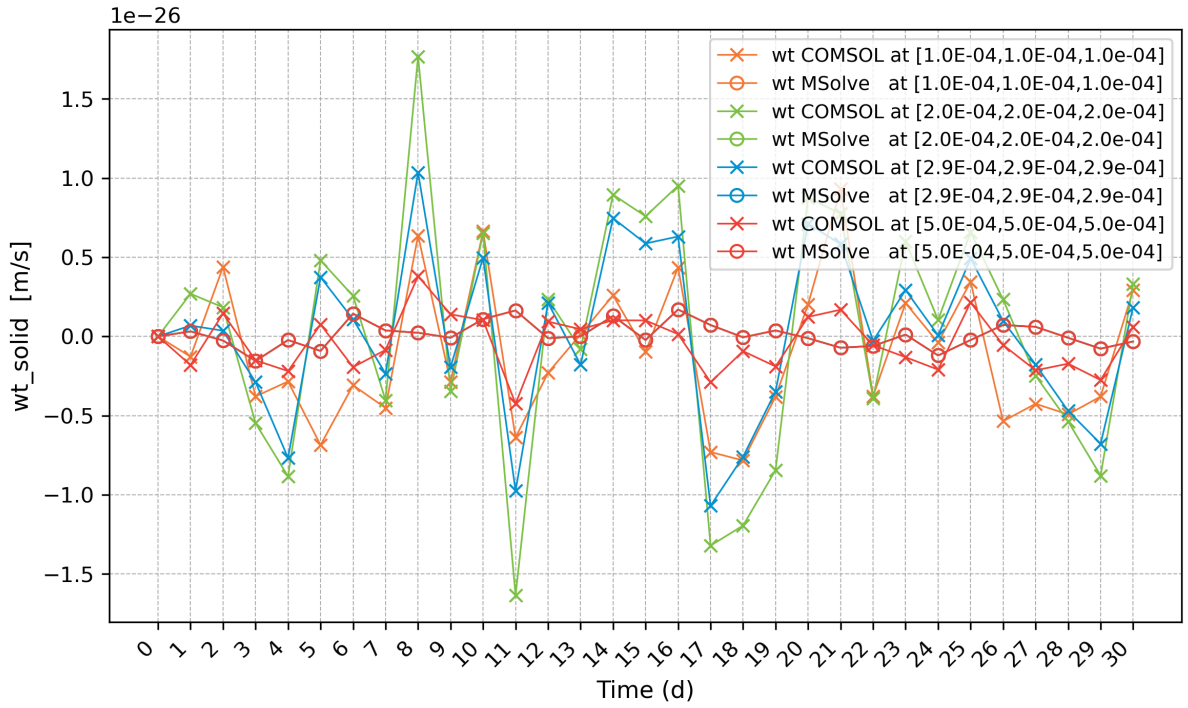

Figure 6.7: Solid Phase Velocity in z-direction over time at the specified nodal coordinates for linear and elastic solid phase tissues.

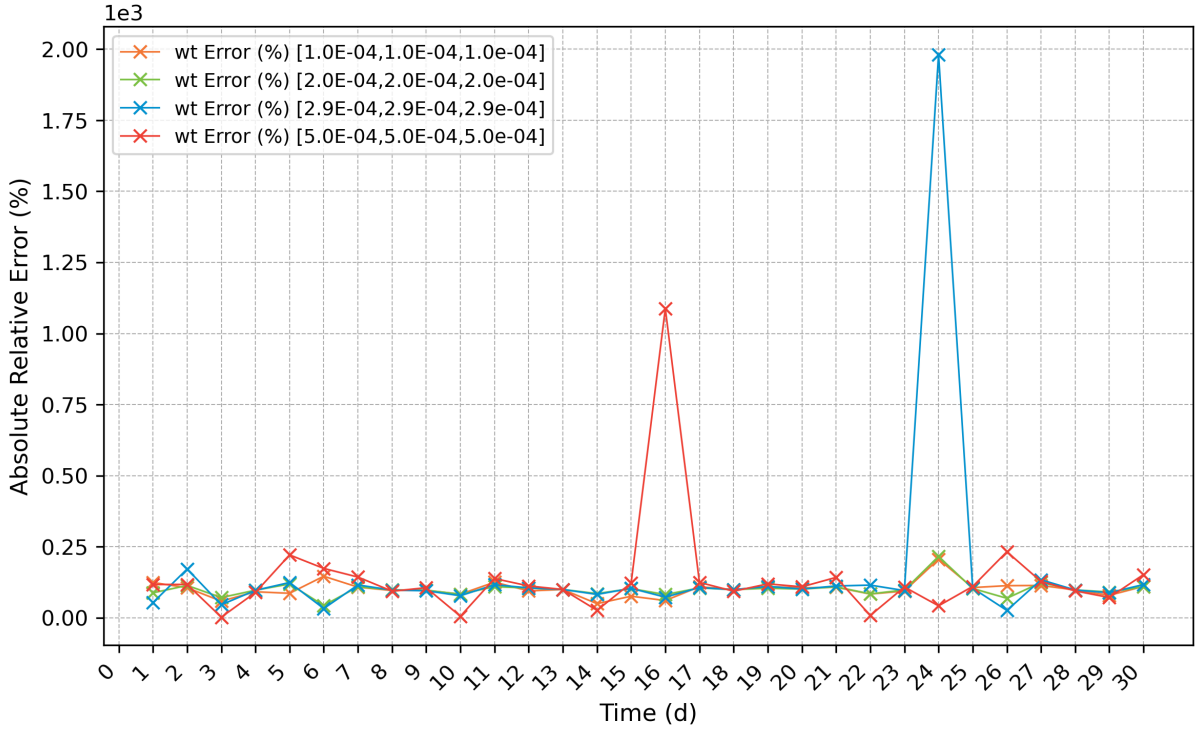

Figure 6.8: Absolute Relative Error (%) of the Solid Phase Velocity in z-direction over time at the specified nodal coordinates for linear and elastic solid phase tissues.

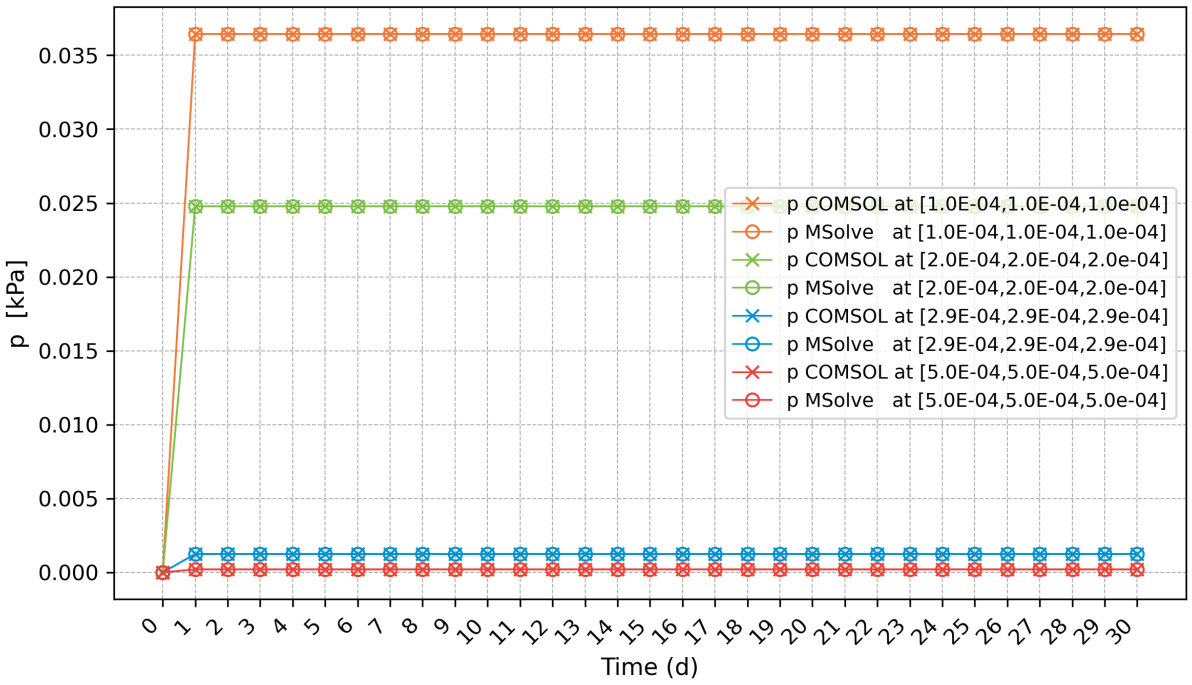

Figure 6.9: Fluid Phase Pressure over time at the specified nodal coordinates for linear and elastic solid phase tissues.

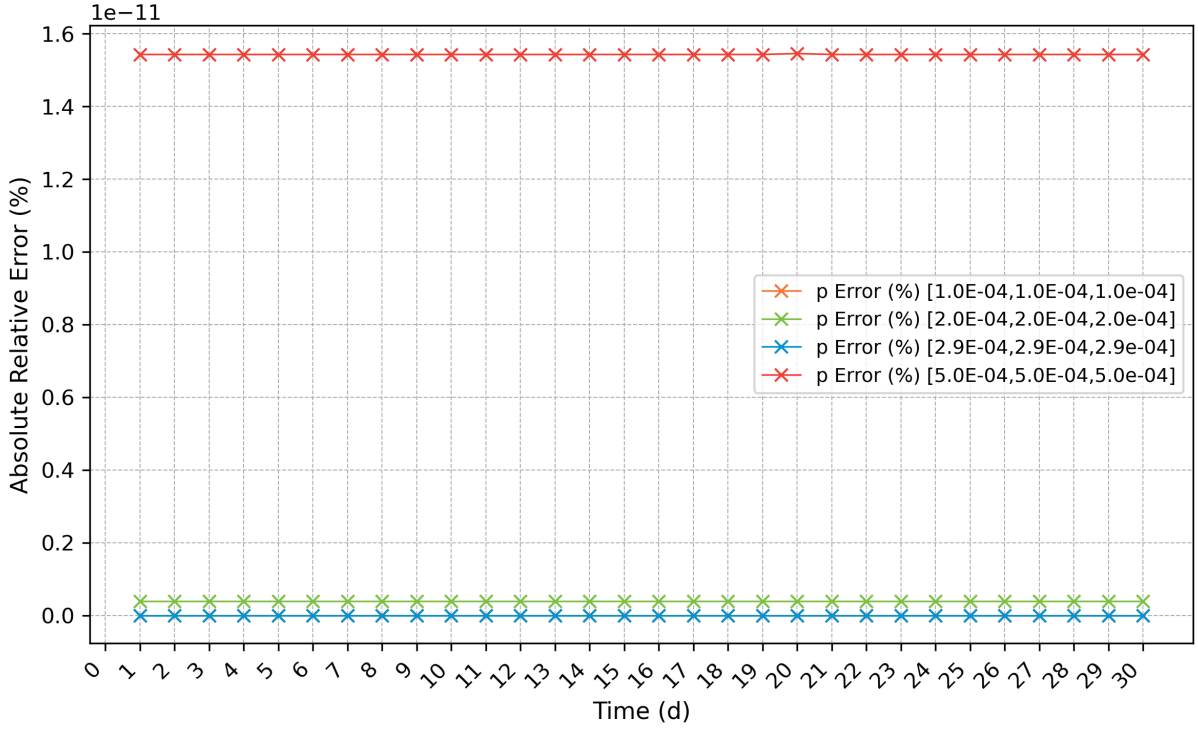

Figure 6.10: Absolute Relative Error (%) of the Fluid Phase Pressure at the specified nodal coordinates for linear and elastic solid phase tissues.

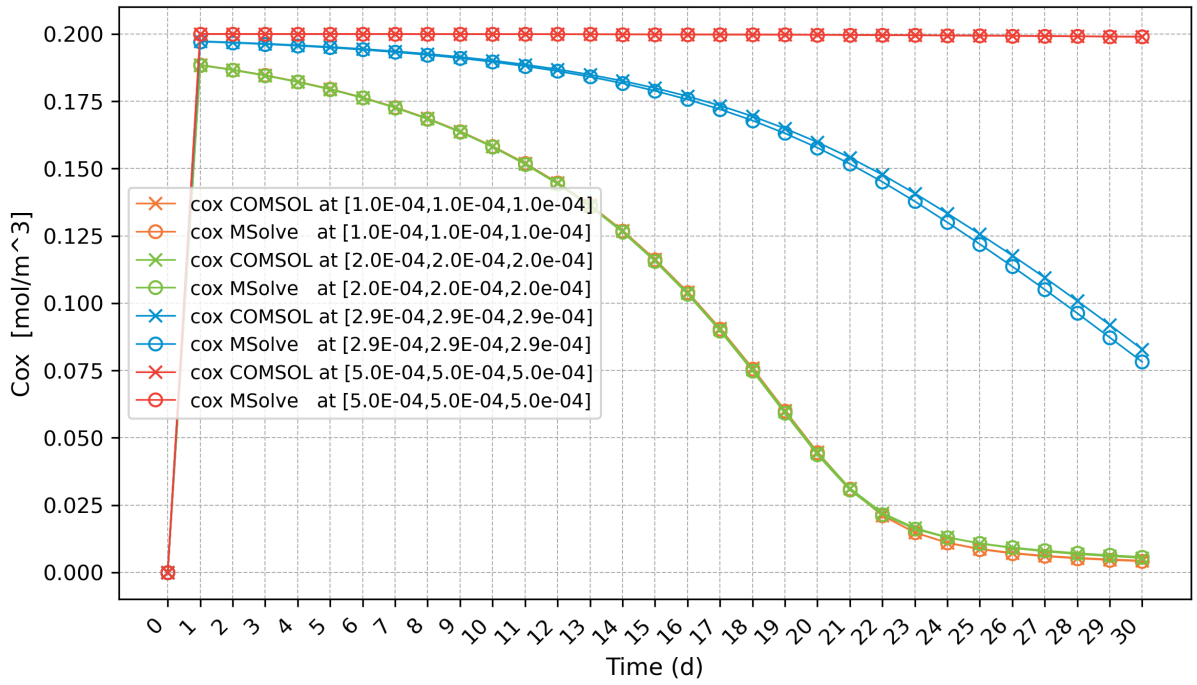

Figure 6.11: Oxygen Concentration over time at the specified nodal coordinates for linear and elastic solid phase tissues.

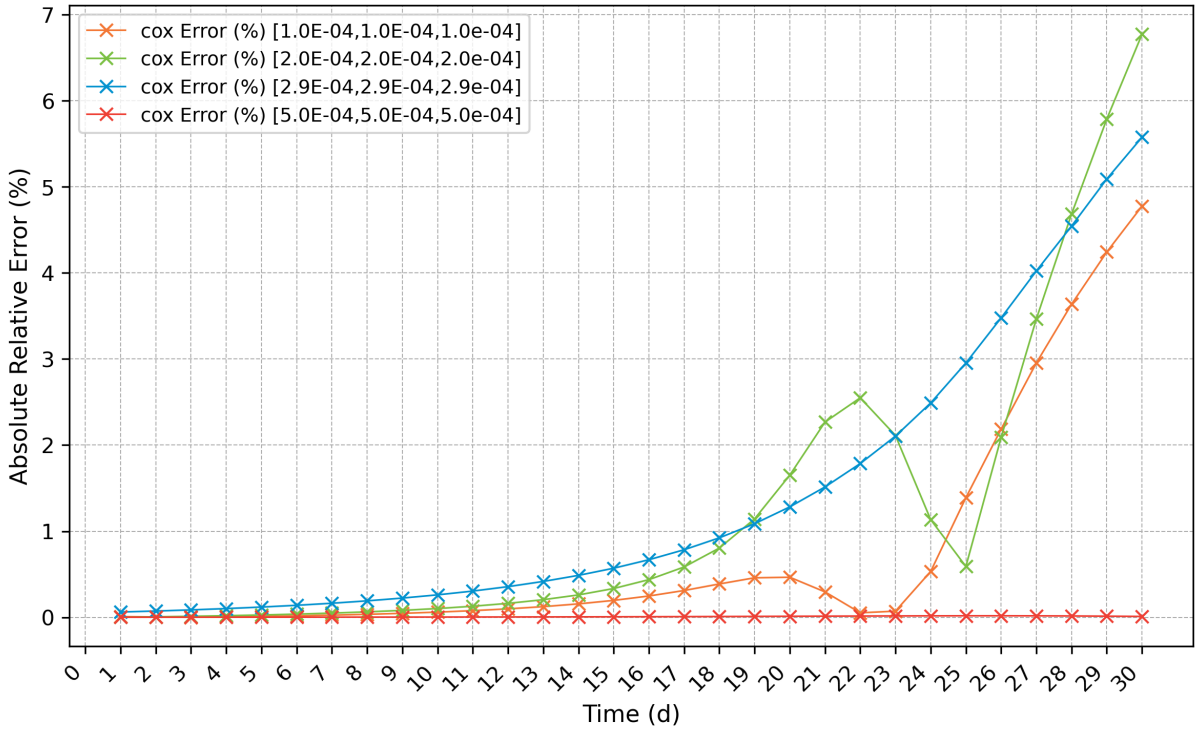

Figure 6.12: Absolute Relative Error (%) of Oxygen Concentration at the specified nodal coordinates for linear and elastic solid phase tissues.

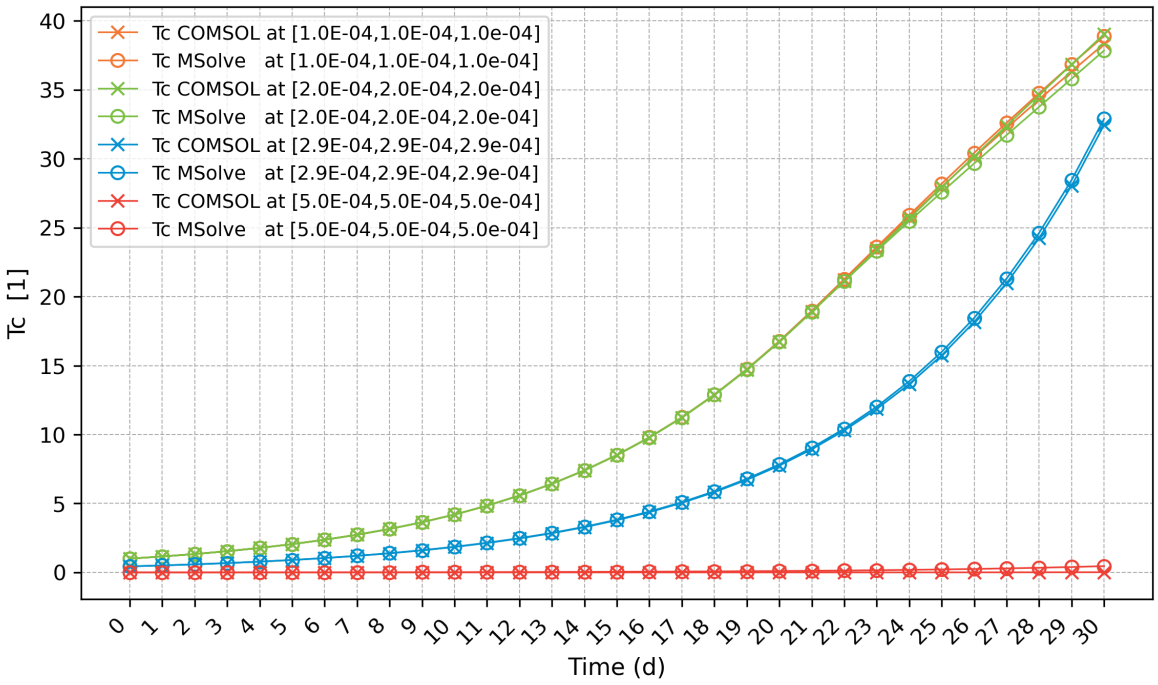

Figure 6.13: Cancer Cell Population over time at the specified nodal coordinates for linear and elastic solid phase tissues.

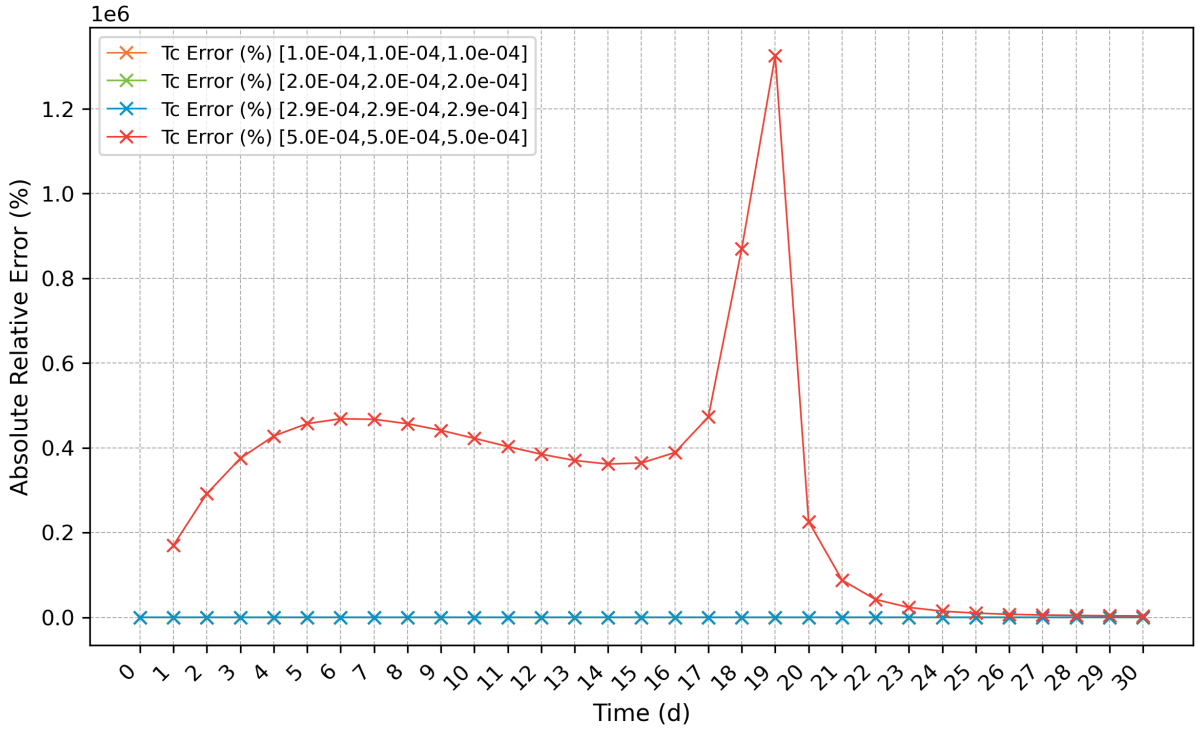

Figure 6.14: Absolute Relative Error (%) of Cancer Cell Population at the specified nodal coordinates for linear and elastic solid phase tissues.

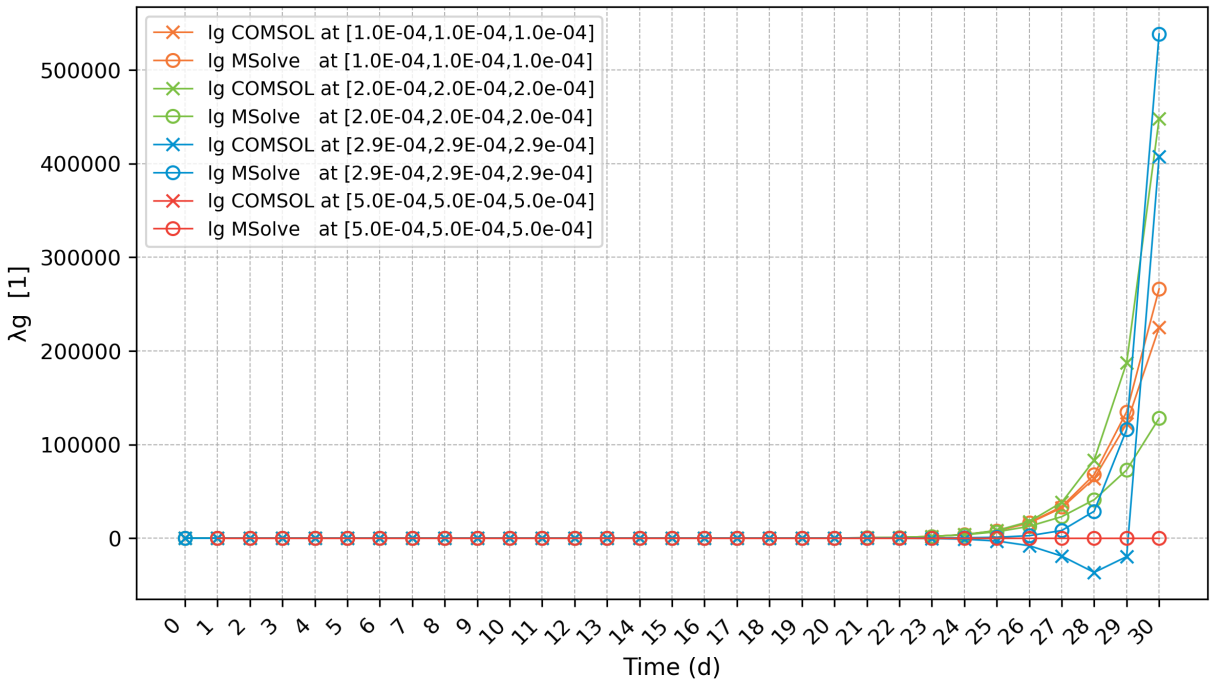

Figure 6.15: Tumor Growth Stretch Ratio over time at the specified nodal coordinates for linear and elastic solid phase tissues.

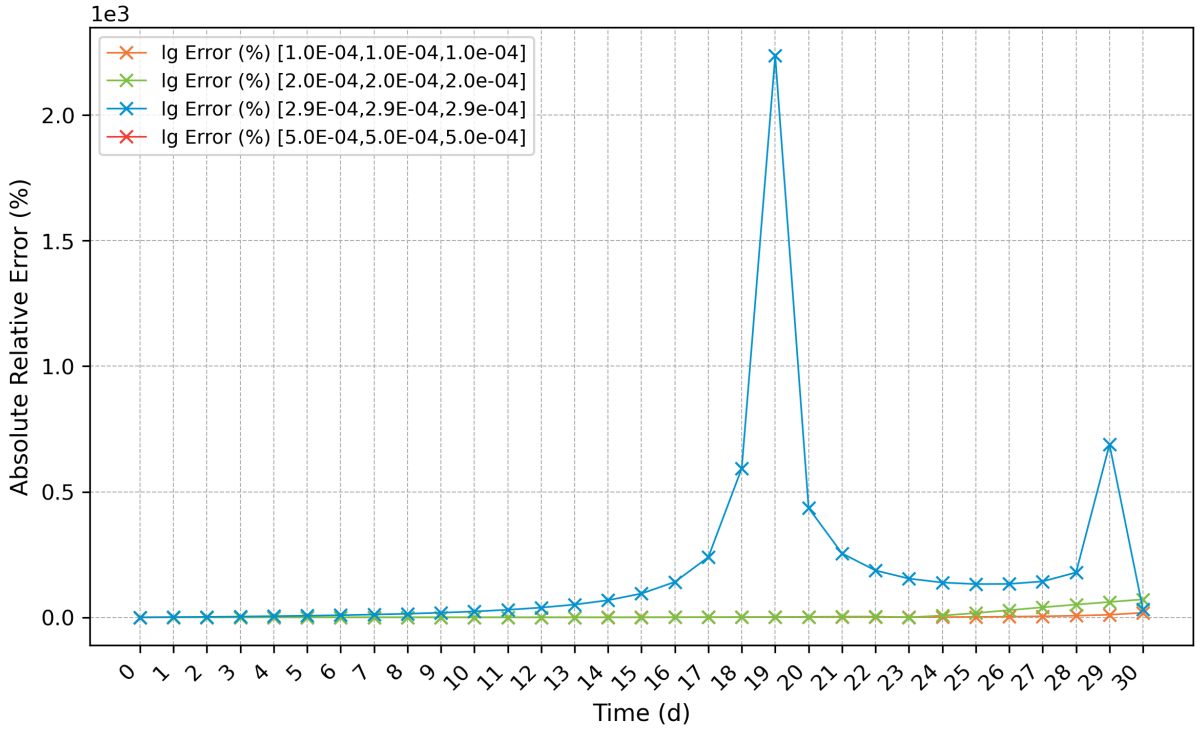

Figure 6.16: Absolute Relative Error (%) of Tumor Growth Stretch Ratio at the specified nodal coordinates for linear and elastic solid phase tissues.

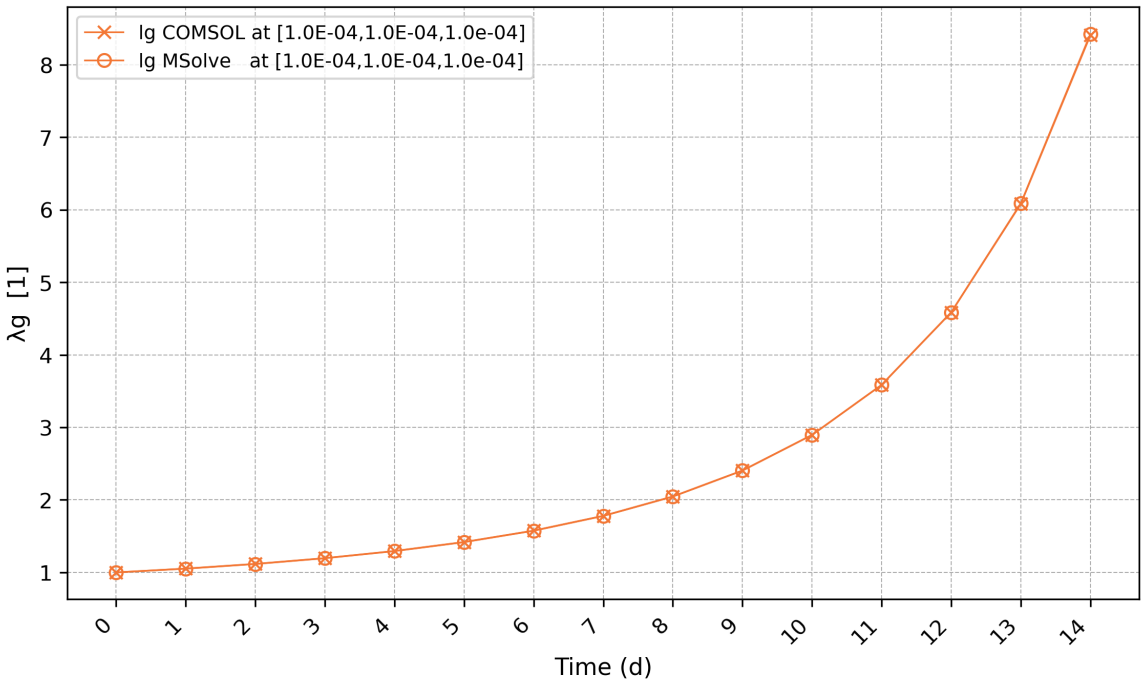

Figure 6.17: Tumor Growth Stretch Ratio over the first 15 days of the analysis at the specified nodal coordinates for linear and elastic solid phase tissues.

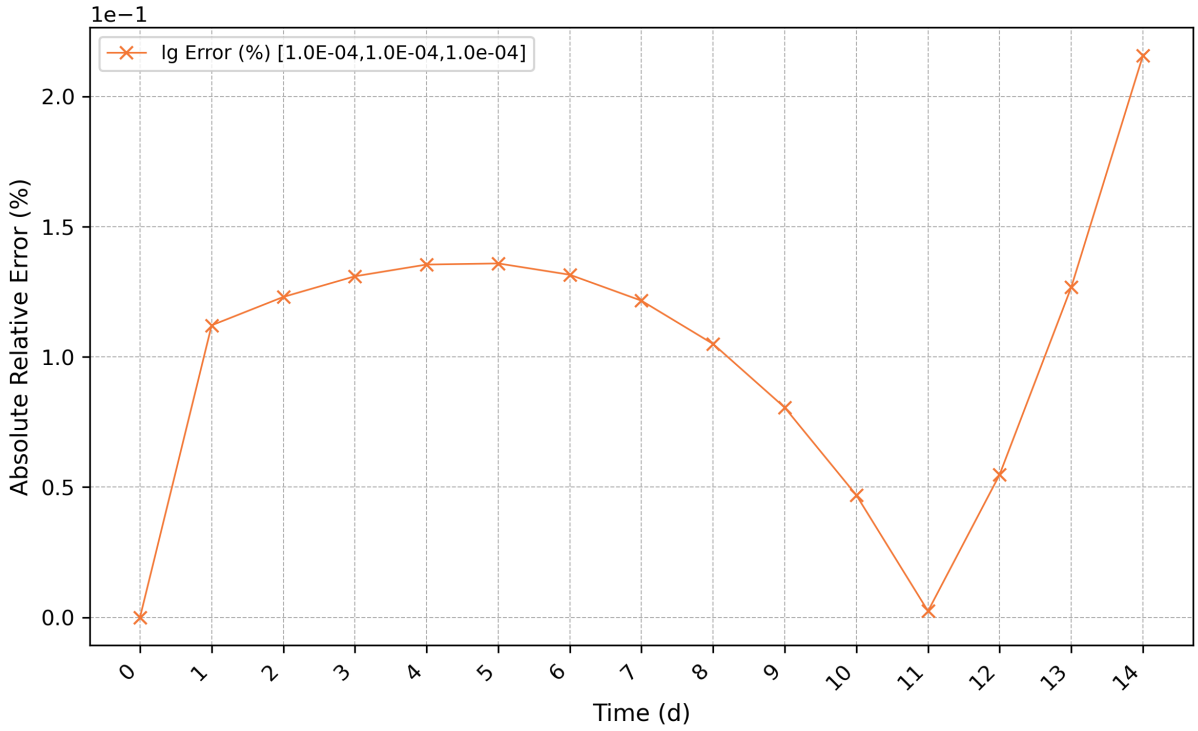

Figure 6.18: Absolute Relative Error (%) of Tumor Growth Stretch Ratio at the specified nodal coordinates for linear and elastic solid phase tissues for the first 20 days of the analysis.

6.3 Numerical Results - Hyperelastic Material

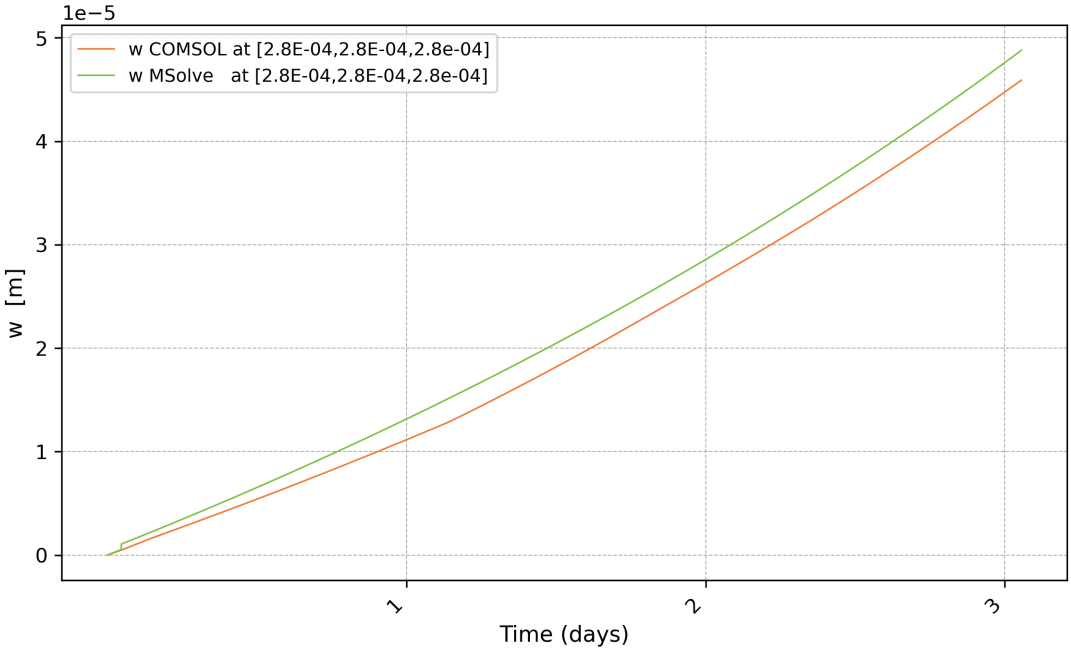

Figure 6.19: Solid Phase Displacement in z-direction over time at the specified nodal coordinates for hyperelastic neo-Hookean solid phase tissues with material and geometry non-linearity.

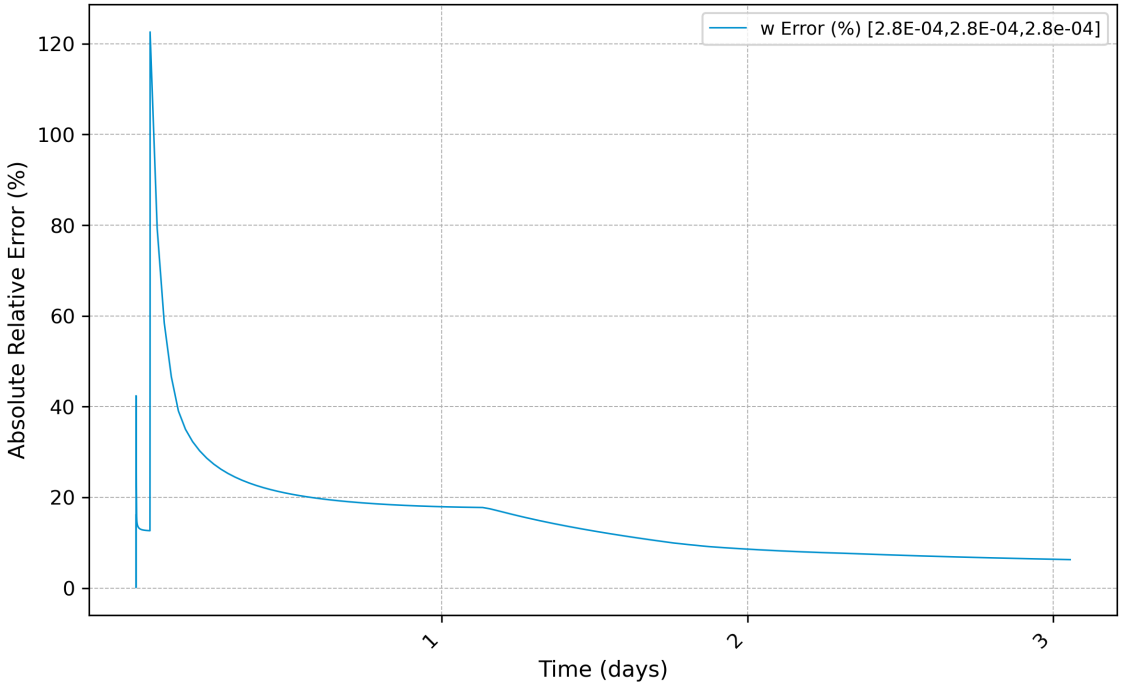

Figure 6.20: Absolute Relative Error (%) of the Solid Phase Displacement in z-direction over time at the specified nodal coordinates for hyperelastic neo-Hookean solid phase tissues with material and geometry non-linearity.

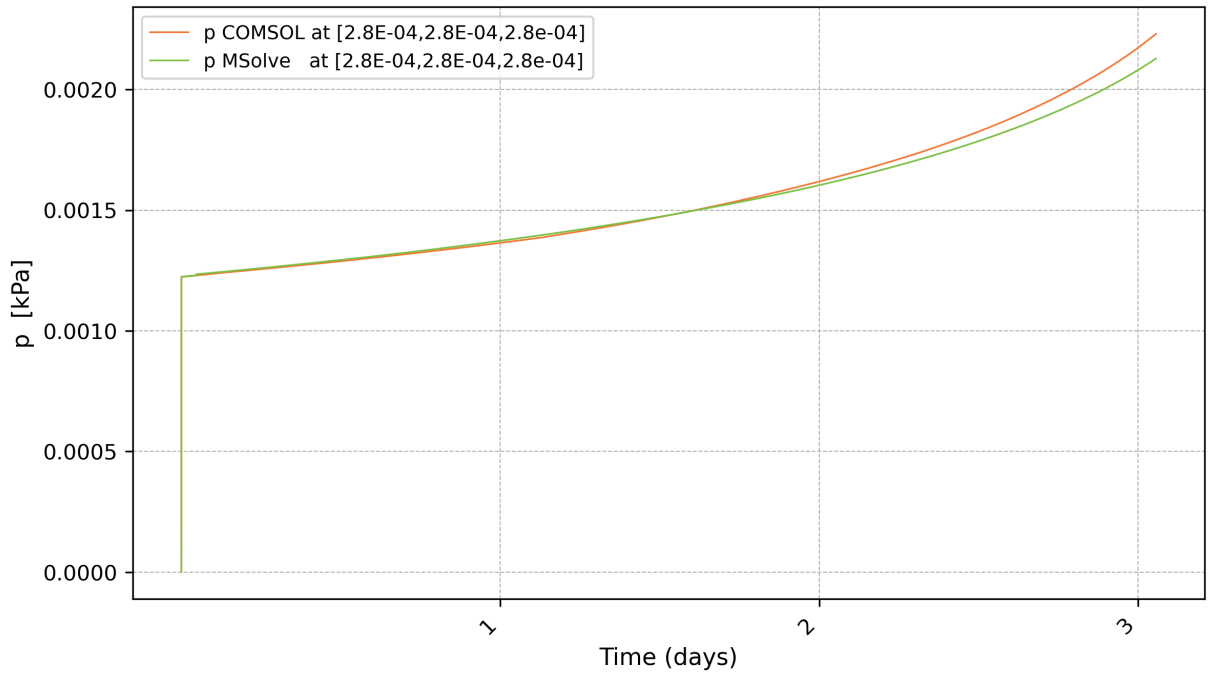

Figure 6.21: Fluid Phase Pressure over time at the specified nodal coordinates for hyperelastic neo-Hookean solid phase tissues with material and geometry non-linearity.

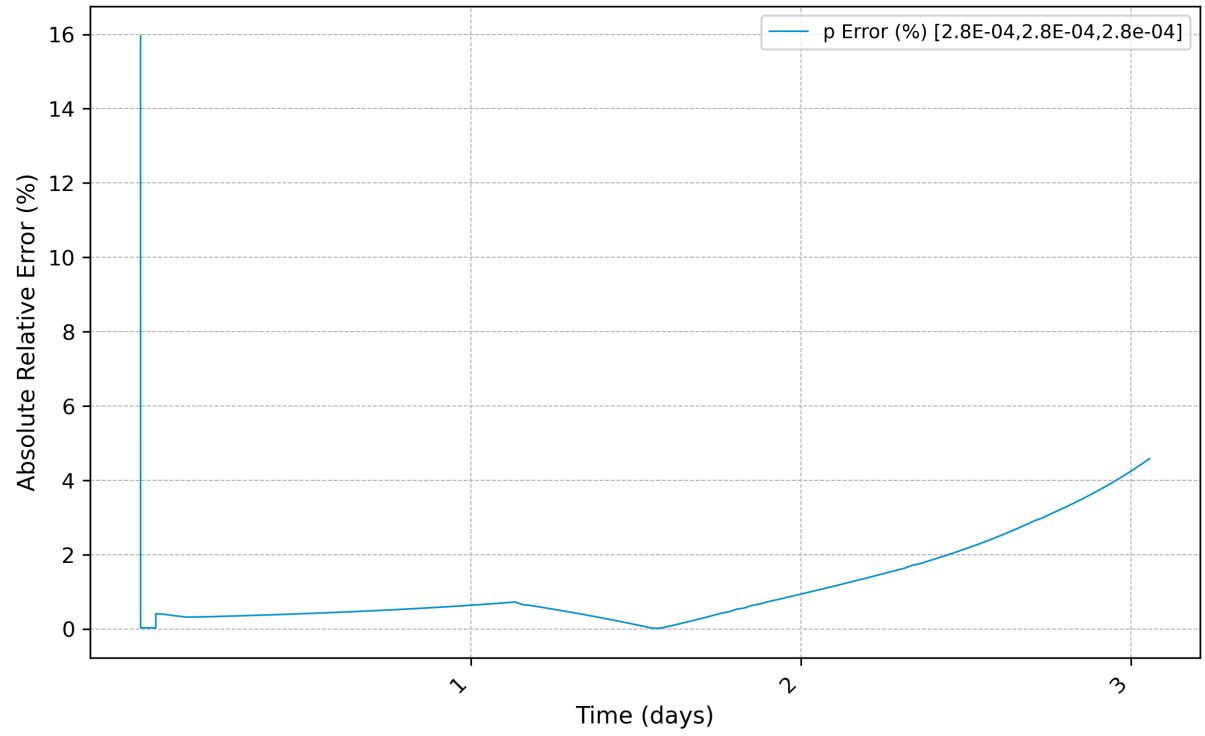

Figure 6.22: Absolute Relative Error (%) of the Fluid Phase Pressure at the specified nodal coordinates for hyperelastic neo-Hookean solid phase tissues with material and geometry non-linearity.

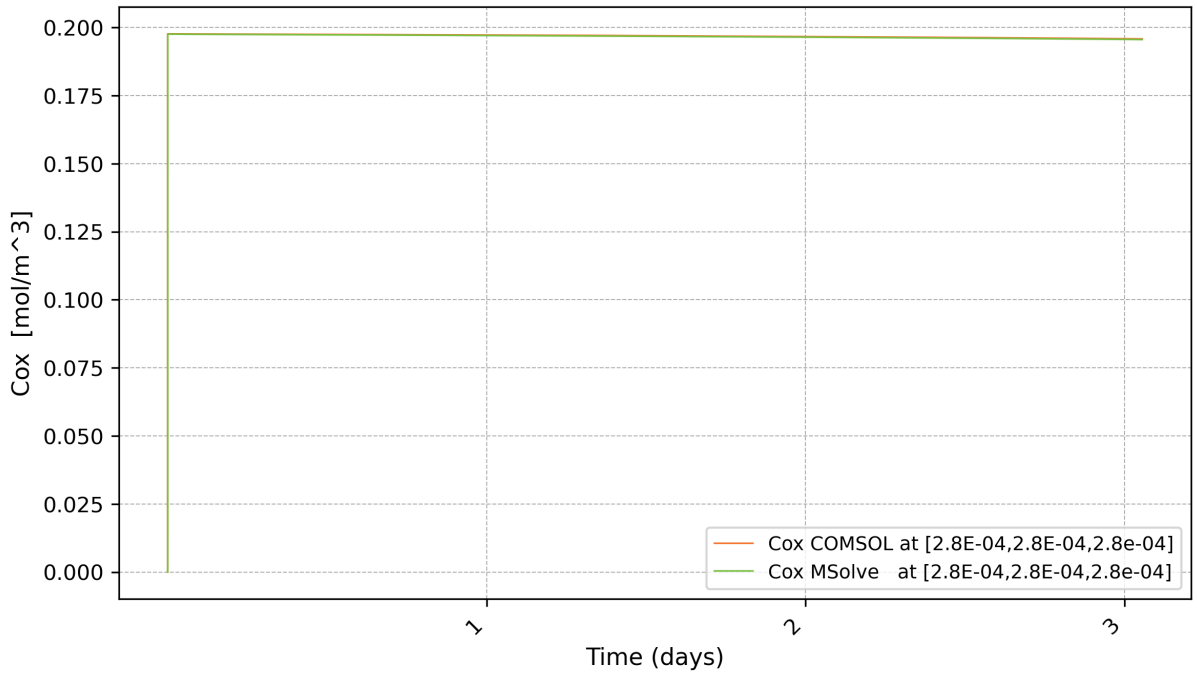

Figure 6.23: Oxygen Concentration over time at the specified nodal coordinates for hyperelastic neo-Hookean solid phase tissues with material and geometry non-linearity.

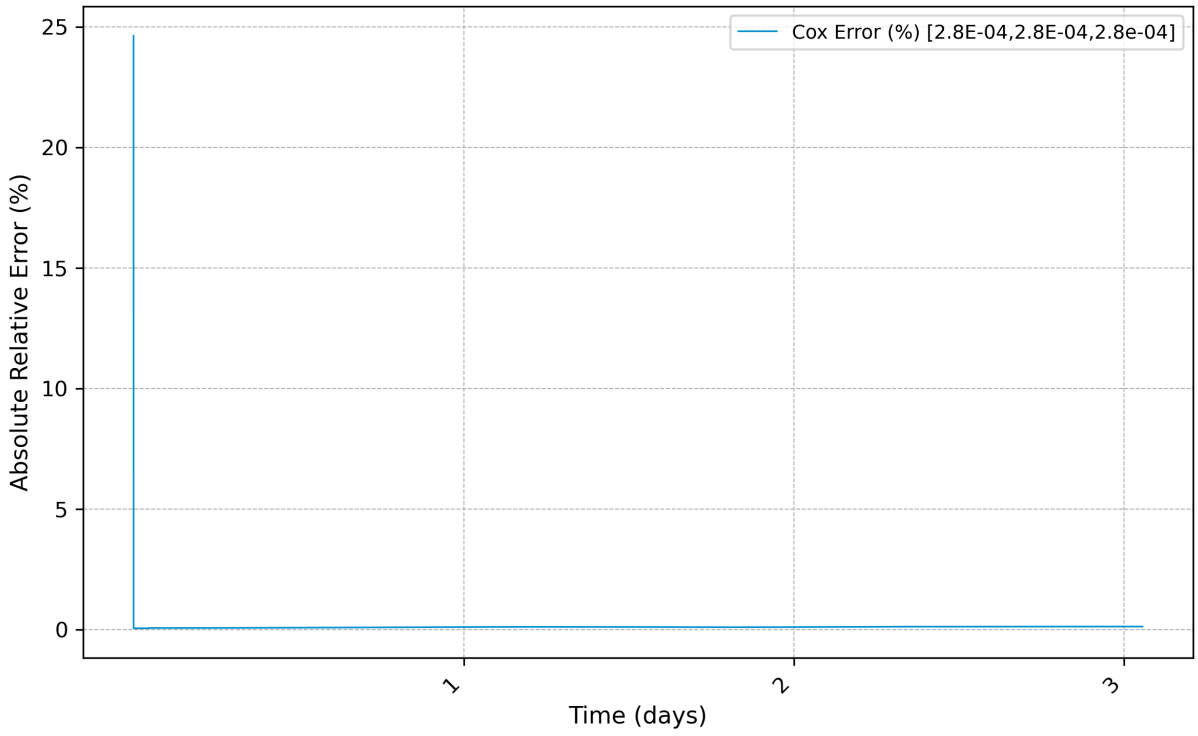

Figure 6.24: Absolute Relative Error (%) of Oxygen Concentration at the specified nodal coordinates for hyperelastic neo-Hookean solid phase tissues with material and geometry non-linearity.

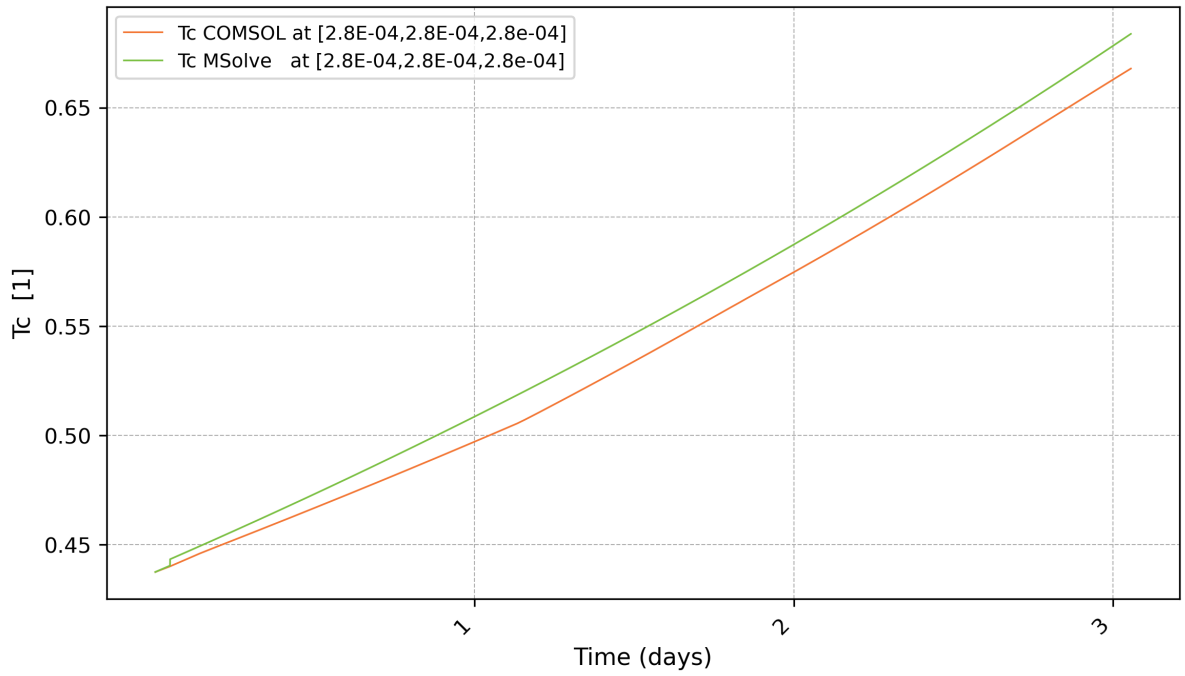

Figure 6.25: Cancer Cell Population over time at the specified nodal coordinates for hyperelastic neo-Hookean solid phase tissues with material and geometry non-linearity.

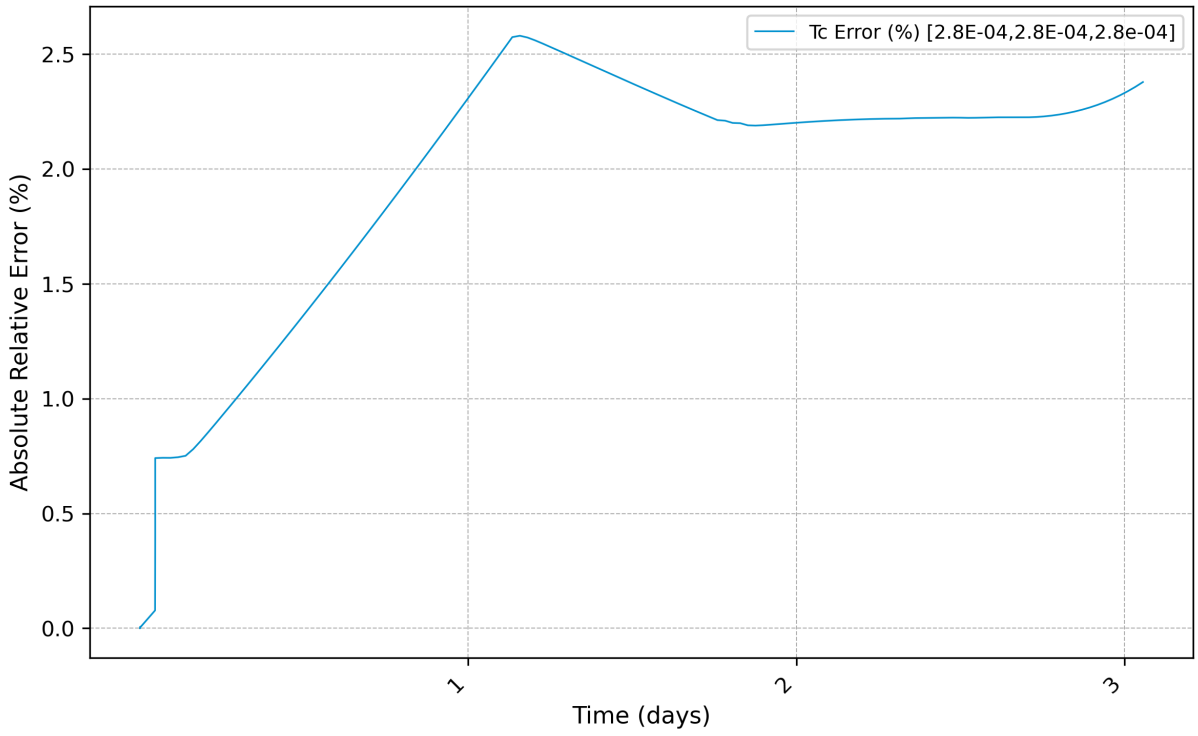

Figure 6.26: Absolute Relative Error (%) of Cancer Cell Population at the specified nodal coordinates for hyperelastic neo-Hookean solid phase tissues with material and geometry non-linearity.

6.4 Discussion & Conclusions

6.4.1 Pressure

Pressure and solid displacements are solved as a single porous medium equation. Equation (2.4) does not include temporal derivatives, but since the divergence of the solid phase velocity is included as a source term, solid displacements over time lead to variations in the pressure field. As it can be seen by Figure 6.10 and Figure 6.22, the solution obtained by MSolve is in perfect agreement with COMSOL, with steady absolute errors over time reaching maximum value around $1.55E-11$ at $(x, y, z) = (5E-4, 5E-4, 5E-4)$. The transient response of the interstitial fluid pressure for of the linear material, reaches it's equilibrium state during the first day at all examined nodes. Transient phenomena seem to smooth out after some seconds and by considering the slow evolving nature of the problem, it is safe to say that they have very small effect. Another insight from the observation of the results is that the contribution of the divergence of the solid velocities field is time-step dependent. In the case of the hype-elastic material, pressure tends to increase slightly with time but there are not sufficient data for it's response over larger time periods like weeks and months.

6.4.2 Displacements

The response is examined under different material constitutive laws. For all cases considered MSolve results are extremely accurate in comparison with the corresponding COMSOL results. For the linear and elastic material where the deformation due to the growth rate is neglected it can be seen at Figures 6.1, 6.3, 6.5 that the solution reaches steady state in the first day of the analysis leading to a zero velocity field, presented in Figure 6.7, that has no effect in the pressure field. The solutions for the solid phase velocity have great error values but this should not be a concern since the values are practically zero. Since pressure does not change over time, its contribution to the stress tensor remains constant. In the case of the hyperelastic material the displacement fields change over time during the examined period and tends to increase since the effect of the tumor growth is considered in the calculations of the strain tensor. The unrestricted growth of the tumor leads to large displacements that deform and may corrupt the elements of the mesh, leading the analysis to fail, since there is a change of sign in the determinant calculated during the isoparametric mapping of the finite element.

6.4.3 Oxygen Concentration & Cancer Cell Population

The results for oxygen and cancer cell population provide a deep insight in their intricate coupling since Equation eq. (2.26) has a non-linear sink term that depends on the population of the cancer cells, while the genesis of cancer cells is tightly associated with oxygen supply. As it can be observed from Figures 6.11, 6.13, oxygen concentration away from the center of the tumor region presents a slight decline that matches with a corresponding increase in the tumor cells in contrast with the regions closer to the axis origins where the response is completely different. The observed node at $(x, y, z) = (2.9E-4, 2.9E-4, 2.9E-4)$ has an exponential increase in tumor cells over time fueled by an oxygen flux that leads to decrease in the local oxygen concentration. Cancer cells increase even more rapidly at the two nodes close to the center of the tumor region with a steep decline of oxygen concentration. During the last 5 days of the analysis, hypoxic conditions appear in the center of the tumor where the oxygen concentration tends to zero and the infected tissue is lead to necrosis. It should be noted that the results for the population of the cancer cells during the last 14 days of the analysis are heavily influenced by an extreme increase in the growth stretch ratio, where while the calculated values are numerically valid, they do not correspond to a biological system

6.4.4 Tumor growth rate

The results for the tumor growth rate, in the case of linear elastic material, exhibit an exponential behavior directly linked to the exponential increase in T_{cc}. Since the effect of growth on the strain tensor is neglected, the displacement fields reach a steady state, regardless of the rapid increase in growth. In the case of hyperelastic tissues, where λ_g is considered in strain calculations, its effects become apparent.

6.4.5 Conclusions

This thesis presented a detailed mathematical model of tumor growth, capturing the intricate dynamics of the tumor micro-environment (TME). The model's biphasic approach, incorporating both solid and fluid phases, reflects the complex interplay within tumor tissues. Through a single porous medium equation, the model closely correlates pressure and solid displacements. Its alignment with COMSOL simulations is evident.

The model adeptly simulates displacements across various material constitutive laws. In linear and elastic materials, the impact of growth rate on deformation is not considered, while hyperelastic materials exhibit time-dependent displacement fields affected by tumor growth.

A critical insight from the model is the interdependency of oxygen concentration and cancer cell population. The non-linear dynamics within tumor regions reveal a mutual dependence, particularly under hypoxic conditions and in areas of rapid tumor cell increase. This underscores the model's biological accuracy.
The predictions on tumor growth rate, especially concerning linear elastic and hyperelastic materials, highlight the essential role of the growth stretch ratio in tumor evolution.
The mathematical model developed in this thesis offers a comprehensive and accurate portrayal of tumor growth and its microenvironment. The simulations' alignment with established software benchmarks instills confidence in the model's predictive capabilities. This work significantly advances our understanding of tumor mechanics and lays a foundation for future cancer treatment research.

6.5 Future Goals

The next phase for the computational model involves leveraging MSolve in conjunction with AI-enhanced numerical methods, aimed at improving the simulation of transport phenomena in tumor areas and refining clinical research parameters for patient-specific cancer immunotherapy treatments.

6.5.1 Integration with AI Tools

The integration of MSolve with AI-Solve and Korali is planned to enable more efficient computation and simulation of complex mechanical systems across various applications. This integration seeks to harness the capabilities of exascale computing, a significant step in computational science.

6.5.2 Utilization of MRI Data

A key future application involves using MRI data from cancer patients to generate finite element meshes. This process aims to provide a more accurate representation of the tumor microenvironment, essential for patient-specific modeling. Korali will be instrumental in optimizing input clinical research parameters, aligning the simulations more closely with clinical realities.

6.5.3 Simulation on Advanced HPC Platforms

Simulations are proposed to be conducted on the Piz Daint supercomputer using MSolve. This approach is expected to offer enhanced computational power and accuracy, facilitating

more detailed and comprehensive analyses.

6.5.4 Statistical Analysis and Bayesian Inference

The computational model will be used to define constraints for surrogate model parameters. Korali will perform statistical analysis and Bayesian inference to validate and refine the model outputs. This step is critical in ensuring the reliability and applicability of the simulation results.

6.5.5 Objective

The overarching goal is to improve the accuracy and applicability of simulations in cancer research, particularly in the realm of personalized cancer treatments. This involves a careful balance of advanced computational techniques, patient-specific data, and rigorous analytical methods, all aimed at enhancing the understanding and treatment of cancer.

Bibliography

[1] *A compendium of mutational cancer driver genes*. Nature. 2023. URL: https://www.nature.com/articles/s41586-019-1186-3.

[2] N. Aravas. "Material Mechanics Körper". In: (2014).

[3] Klaus-Jurgen Bathe. "Finite Element Procedures Körper". In: (2014), pp. 485–642.

[4] Klaus-Jurgen Bathe. "Finite Element Procedures Körper". In: (2014), pp. 777–779.

[5] The BMJ. "Global cancer cases and deaths are set to rise by 70% in next 20 years". In: (2021).

[6] H. Byrne and L. Preziosi. "Modelling solid tumour growth using the theory of mixtures". In: *Mathematical Medicine and Biology* 20 (2003), pp. 341–366.

[7] *Cancer-Causing Substances in the Environment*. National Cancer Institute. 2023. URL: https://www.cancer.gov/about-cancer/causes-prevention/risk/substances.

[8] J.J. Casciari, S.V. Sotirchos, and R.M. Sutherland. "Mathematical modeling of microenvironment and growth in EMT6/Ro multicellular tumor spheroids". In: *Cell Proliferation* 25 (1992), pp. 1–22.

[9] V.P. Chauhan et al. "Angiotensin inhibition enhances drug delivery and potentiates chemotherapy by decompressing tumour blood vessels". In: *Nature Communications* 4 (2013).

[10] G. Cheng et al. "Micro-environmental mechanical stress controls tumor spheroid size and morphology by suppressing proliferation and inducing apoptosis in cancer cells". In: *PLoS ONE* 4 (2009).

[11] J. Chung and G.M. Hulbert. "A time integration algorithm for structural dynamics with improved numerical dissipation: The generalized- method Körper". In: *Journal of Applied Mechanics* 60 (1993), pp. 371–375.

[12] *Environmental Factors in Cancer Development*. Encyclopedia.com. 2023. URL: https://www.encyclopedia.com/food/news-wires-white-papers-and-books/environmental-factors-cancer-development.

[13] E. Theotokoglou Körper G. Tsamasfiros. "Finite Elements Mehtod". In: (2014).

[14] *Genetic Mutations*. American Cancer Society. 2023. URL: https://www.cancer.org/cancer/cancer-causes/genetics/understanding-genetic-testing-for-cancer.html.

[15] "Global Cancer Statistics 2020: GLOBOCAN Estimates of Incidence and Mortality Worldwide for 36 Cancers in 185 Countries". In: *CA: a cancer journal for clinicians* 71.3 (2021). Available: https://pubmed.ncbi.nlm.nih.gov/33538338/, pp. 209–249.

[16] G. Griffon-Etienne et al. "Taxane-induced apoptosis decompresses blood vessels and lowers interstitial fluid pressure in solid tumors: clinical implications". In: *Cancer Research* 59 (1999), pp. 3776–3782.

[17] G. Helmlinger et al. "Solid stress inhibits the growth of multicellular tumor spheroids". In: *Nature Biotechnology* 15 (1997), pp. 778–783.

[18] H.M. Hilber, T.J.R. Hughes, and R.L. Taylor. "Improved numerical dissipation for time integration algorithms in structural dynamics". In: *Earthquake Engineering and Structural Dynamics* 5 (1977), pp. 283–292.

[19] *Impact of Gene–Environment Interactions on Cancer Development*. PubMed Central (PMC). 2023. URL: https://www.ncbi.nlm.nih.gov/pmc/articles/PMC6220006/.

[20] R.K. Jain. "Normalizing tumor microenvironment to treat cancer: bench to bedside to biomarkers". In: *Journal of Clinical Oncology* 31 (2013), pp. 2205–2218.

[21] R.K. Jain, J.D. Martin, and T. Stylianopoulos. "The role of mechanical forces in tumor growth and therapy". In: *Annual Review of Biomedical Engineering* 16 (2014), pp. 321–346.

[22] Y. Kim, M.A. Stolarska, and H.G. Othmer. "The role of the microenvironment in tumor growth and invasion". In: *Progress in Biophysics and Molecular Biology* 106 (2011), pp. 353–379.

[23] J. MacLaurin et al. "The buckling of capillaries in solid tumours". In: *Proceedings of the Royal Society A: Mathematical, Physical and Engineering Sciences* 468 (2012), pp. 4123–4145.

[24] V.C. Mow et al. "Biphasic creep and stress-relaxation of articular-cartilage in compression: Theory and experiments". In: *Journal of Biomechanical Engineering* 102 (1980), pp. 73–84.

[25] F. Mpekris et al. "Stress-mediated progression of solid tumors: effect of mechanical stress on tissue oxygenation, cancer cell proliferation, and drug delivery". In: *Biome-*

chanics and Modeling in Mechanobiology 14.6 (2015), pp. 1391–1402. DOI: 10.1007/s10237-015-0682-0.

[26] N.M. Newmark. "A method of computation for structural dynamics". In: *Journal of the Engineering Mechanics Division* 85 (1959), pp. 67–94.

[27] T.P. Padera et al. "Cancer cells compress intratumour vessels". In: *Nature* 427 (2004), p. 695.

[28] *Risk Factors for Cancer*. MSD Manual Consumer Version. 2023. URL: https://www.msdmanuals.com/home/cancer/risk-factors-for-cancer/environmental-factors.

[29] E.K. Rodriguez, A. Hoger, and A.D. McCulloch. "Stress-dependent finite growth in soft elastic tissues". In: *Journal of Biomechanics* 27 (1994), pp. 455–467.

[30] T. Roose et al. "Solid stress generated by spheroid growth estimated using a linear poroelasticity model". In: *Microvascular Research* 66 (2003), pp. 204–212.

[31] T. Stylianopoulos et al. "Coevolution of solid stress and interstitial fluid pressure in tumors during progression: implications for vascular collapse". In: *Cancer Research* 73 (2013), pp. 3833–3841.

[32] T. Stylianopoulos et al. "Permeability calculations in three-dimensional isotropic and oriented fiber networks". In: *Physics of Fluids* 20 (2008), p. 123601.

[33] L.A. Taber. "Theoretical study of Beloussov's hyper-restoration hypothesis for mechanical regulation of morphogenesis". In: *Biomechanics and Modeling in Mechanobiology* 7 (2008), pp. 427–441.

[34] *The Genetics of Cancer*. National Cancer Institute. 2023. URL: https://www.cancer.gov/about-cancer/causes-prevention/genetics.

[35] "The global burden of cancer: priorities for prevention". In: *Carcinogenesis* 31.1 (2010). Available: https://www.ncbi.nlm.nih.gov/pmc/articles/PMC2802672/, pp. 100–110.

[36] UICC. *GLOBOCAN 2020: New Global Cancer Data*. https://www.uicc.org/news/globocan-2020-new-global-cancer-data. 2020.

[37] C. Voutouri and T. Stylianopoulos. "Evolution of osmotic pressure in solid tumors". In: *Journal of Biomechanics* 47 (2014), pp. 3441–3447.

[38] G. Xu, P.V. Bayly, and L.A. Taber. "Residual stress in the adult mouse brain". In: *Biomechanics and Modeling in Mechanobiology* 8 (2009), pp. 253–262.

[39] G. Xu et al. "Opening angles and material properties of the early embryonic chick brain". In: *Journal of Biomechanical Engineering* 132 (2010), p. 011005.